DESIGN, CONSTRUCTION, AND IMPLEMENTATION OF IONIZATION METHOD SURFACE POTENTIAL INSTRUMENT FOR STUDIES OF CHARGED SURFACTANTS AND INORGANIC ELECTROLYTES AT THE AIR/WATER INTERFACE

THESIS

Presented in Partial Fulfillment of the Requirements for the Degree Master of Science in the Graduate School of The Ohio State University

By

Tehseen Adel

Graduate Program in Chemistry

The Ohio State University

2017

Master's Examination Committee:

Dr. Heather C. Allen, Advisor

Dr. Anne Co

Copyrighted by

Tehseen Adel

2017

Abstract

Surface potential is a valid and relevant macroscopic technique used to determine the orientation of water dipoles at the interface of air and water. In this work, an ionization based surface potential (SP) instrument is designed and configured. The first set of results are presented here. A custom designed americium-gold matrix foil with an activity of 20μCi and 9.5mm surface diameter is used as the air electrode suspended over a sample solution. A parallel aligned platinum gauze electrode is immersed in solution directly under the probe. The electrodes are connected to a Keithley 6517B electrometer. Subsequent measurements are made in the DC voltage mode of the electrometer for charged surfactants (SDS, CTAB) and inorganic electrolytes (NaCl, $MgCl_2$, Na_2SO_4, $MgSO_4$). The surface potential measurements were compared to studies by Nakahara et. al, (2005, 2008) and Jarvis and Scheiman (1968).

The potentials measured for SDS showed linear increase from 1 to 5mM consistent with previous findings in that regime. A similar result is observed with CTAB in the 0.8-1mM concentration regime. The measured sign of the potentials is consistent with the sign of the surface charge for these molecules. For the inorganic salts, the surface potential difference is plotted versus concentration. Though the magnitude of these results does not fall within range of the Jarvis-Scheiman study, similar trends are observed. Positive trends are observed for Na_2SO_4 and $MgSO_4$ and negative trends for NaCl and $MgCl_2$. These results are compared to several MD simulation studies which show the surface propensity for ions and its effect on the electric double layer.

The results of this study are key to validating observations of measurements using macroscopic techniques for air/water interface studies. Knowledge gained from these studies will provide insight into questions regarding multiple aqueous ion studies: atmospheric aerosol chemistry, thundercloud electrification, geochemistry, ocean surface processes, etc.

Dedication

To my family who have supported me with everything.

Acknowledgments

Thank you to Dr. Heather Allen for all the support and assistance she provided. I would like to thank members of the Allen group, especially Cathryn Schoeppner and Ka Chon Ng for their help with this project in the lab. This project would have been almost impossible to complete without the assistance of Eric Jackson and others at the Computer Instrument Support Group. Thank you!

Vita

May 2015……. B.S. Chemistry, Cedarville University

2015 to present…… Graduate Teaching Associate, Department of Chemistry, The Ohio State University

Fields of Study

Major Field: Chemistry

Table of Contents

List of Tables

List of Figures

Abbreviations

α	phase alpha
β	phase beta
i	chemical species
c	concentration
z	charge number of an ion
N_A	Avogadro constant
k	Boltzmann constant
F	Faraday constant
μ	chemical potential
$\tilde{\mu}$	effective chemical potential or electrochemical potential
Δ	change in or relative quantity
ψ	outer potential
φ	inner potential
χ	surface or chi-potential
ϕ	measured inner potential difference
E	measured surface potential
ΔV	measured surface potential relative to pure subphase
$\mu_\perp$	normal component of dipole moment
$\boldsymbol{\varepsilon}_0$	permittivity of free space
$\boldsymbol{\varepsilon}_r$	relative permittivity of a medium
κ	reciprocal Debye length
ρ	charge density of a point
σ	surface charge density
γ	surface tension

Chapter 1 INTRODUCTION

1.1 Overview

In this work, a refined analytical surface potential (SP) instrument was built with the first set of results presented in the thesis. Other aspects of this thesis summarize the theory and experimental aspects of SP. Ultimately, surface potential is an important macroscopic technique in understanding the interfacial behavior of molecules at the air/water interface. Unlike surface tension, surface potential provides insight in molecular or ionic interaction with interfacial water, particularly the "flip-flop" orientation of water dipoles[1] with respect to interacting species.

Chapter 1 summarizes the relevance of understanding ion behavior at the air/water interface and includes a discussion of the historical perspectives and much more recent findings. Chapter 2 includes the theories considered with respect to electrical phenomena of the air/water interface. Chapter 3 forms the crux of this thesis where the combination of theory and experimental considerations allow for the optimal design, construction, and implementation of SP. Chapters 4 and 5 outline the experiment and results. This thesis outlines its conclusions in Chapter 6 with a discussion on future studies with this instrument.

1.2 Motivations

1.2.1 Ubiquity of ions at the aqueous interface

Electrolytes at interfaces have a critical impact in a wide variety of fields, including physical, chemical, biological, and atmospheric studies. An accurate characterization of ion behavior serves as the fundamental basis for knowledge. There are several illustrative examples

of the applicability of ion response at the interface. For instance, there is a biological implication of macromolecular structures stabilized by specific ions, i.e., the lyotropic series. Aqueous ions at the hydrophobic biopolymer-water interface promote degrees of stability to proteins.[2,3] Similarly, interactions based on the ion specificity also extend to other biophysical systems: (1) Ion interactions with colloid particles in solution.[4] (2) Stabilization of micelles, vesicles, and other amphiphilic aggregates in salt solutions.[5]

Another instance of an insufficient understanding of surface ion behavior is the role of aqueous ions at the seawater-ice interface in the polynyas at Earth's poles, which bear major geological and climatological ramifications.[6] As a natural phenomenon, brine rejection occurs when salt is pushed from forming ice, into the surrounding seawater, creating traps of dense and concentrated brine within the sea ice.[7] The increased density of the underlying water masses acts as a trigger of massive ocean circulations which influence global climate. An analogous mechanism of brine rejection also occurs as super cooled cloud water droplets freeze upon impact since salt ions are present in soluble cloud condensation nuclei. This has been suggested as a mechanism for thundercloud electrification, where charge transfer results from collisions between brine covered surfaces of graupel and ice crystals.[8] Within the context of the air/water interface, however, aqueous ion response is hardly understood and the discovery will be more impactful for technological and environmental processes.

1.2.2 A historical perspective

Over the past 130 years, the effect of electrolytes on the air/water interface has been subject to intense study. While bulk properties of electrolytes have been reviewed thoroughly,

behavior of ions at interface is a new frontier of study. In 1888, Hofmeister observed the effect of electrolytes on the solubility of purified albumen. He noted anions had a larger effect on proteins compared to cations. Several years following this discovery, Heydweiller[9] showed electrolytes in water increased the surface tension of the air/water interface. Cations appeared to show little effect on the surface tension, whereas anions affected it considerably. Indeed, the magnitude of variation of surface tension followed the same sequence as Hofmeister's findings.

In 1917, Langmuir[10] proposed an explanation of the physical nature behind the increase in the surface tension caused by electrolytes. Using Gibbs adsorption isotherm model, Langmuir argued the increase is the result of ion depletion of solute in the surface layer which is proportional to the concentration. In comparing the measurements of potassium chloride solutions, Langmuir concluded the thickness of the adsorbed pure water region is 4Å thick. Others showed the variation of interfacial thickness depended on the concentration of added salts. This established a long-held picture of ions as being devoid at the surface. Expanding on Langmuir's ideas, Wagner[11] incorporated the Debye-Hückel (DH) theory of strong electrolytes to suggest that ionic depletion is caused from electrostatic repulsion from interaction of ions with their "electrostatic images" across the air/water interface. Onsanger and Samaras[12] (OS) argued a simplified version of that theory and derived a limiting law that applied to all electrolytes at a sufficiently low concentration. Experimentally, this limiting law applied well to lower concentrations but not higher ones, where it invariably fails to predict surface tension. Like Langmuir, Wagner and OS incorporated the Gibbs adsorption isotherm equation to obtain the excess surface tension. In 2000, Levin and Flores-Mena[13] introduced a different method based on

calculations of direct Helmholtz free energy. Incorporating Wagner and OS insights, they argued the ionic hydration of ions at the interface led to a repulsion from the Gibbs dividing surface. While their calculations agreed with experimental surface tension values, the model failed to account for ionic specificity, particularly differences between halides salts.

Frumkin[14] (1924) and Randels[15,16] (1957, 1965) measured the electrostatic potential difference (surface potential) of aqueous electrolyte solutions across the air/water interface. Their results confirmed that ions were only repelled from the surface depending upon the individual properties of ions; just as Hofmeister had discovered in his lyotropic series. Both studies argued that anions are preferential to the surface compared to cations, and the anions with the lowest hydration energies are prone to the surface, whereas cations were independent of hydration energy. Additionally, Jarvis and Scheiman[17] (1968) also measured the surface potentials of salt solutions (Figure 1.1). From their analysis, they described the water molecules at the air/water interface to orient in a preferential manner that formed an electrical double layer (EDL).[18]

Solvated anions accumulated in the positively charge innermost portion of the double layer, whereas the outermost part remained negative. The Jarvis and Scheiman study also measured the surface tension of the salts (DuNouy ring; ±0.1mM/m) and observed poor correlation to the surface potential data. The authors emphasized how surface tension values were the result of intermolecular forces of attraction, which is different from the electrical properties of electrolytes at the surface. Surface potential of electrolytes has since been reviewed by Randels[19] (1977) and Durand-Vidal et. al.[20] (2000). Theoretical and experimental results confirmed the consideration of the structure of pure water based on surface potential

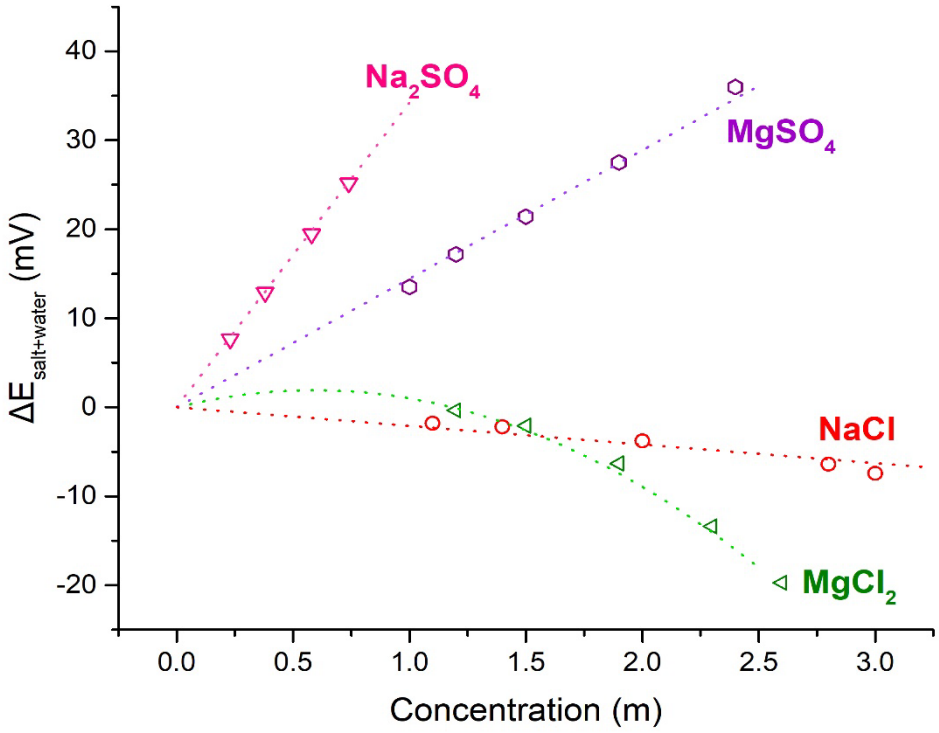

Figure 1.1 Surface potential difference of salts showing the differences of sign and magnitude. Taken from Jarvis and Scheiman, 1968.

measurements carried out by Jarvis and Scheiman. More recently, molecular dynamic (MD) simulations show the asymmetric orientation of water molecules and the effect of this on the free energy profiles for oppositely charged ions. Studies on various halide salts (NaF, NaCl, NaBr, NaI) at the water surface using vibrational sum frequency spectroscopy (VSFG) showed hydrogen bonding of water depended primarily on the anionic species. These key findings eventually led to the molecular dynamic simulation studies by Jungwirth and Tobias[21]. In their model, they proposed large halide ions (Br-, I-) as having high propensity for the surface while ionic distribution in the interface region maintained a negative surface excess. Several

experiments later confirmed that prediction. Levin et. al.[22] (2010) proposed a thermodynamic model in which anions come from a race between the change in cavitation and Born electrostatic energies. While these studies established the tendency of anions to adsorb at the surface, a much clearer scope of its impact emerged only recently.

Dependent on its propensity for the surface, cations and anions redistribute within the interfacial region to form the EDL[23]. Since the EDL itself induces changes in the orientation of interfacial water molecule and the organization of hydrogen-bonding network of water, the interfacial macroscopic properties of surface tension and surface potential is likely to be affected as well[23]. Thus, an investigation of these macroscopic properties is fundamental to understanding the electric properties of electrolytes at the air/water interface.

1.2.3 A more "complex" view of ions at the interface

Knowledge about the molecular-scale interaction of monovalent, multivalent, and complex polyatomic ions at the aqueous interface is incomplete. Close to a decade ago, the understanding of interfacial charge separation from dissolution of electrolytes was relatively simplistic as most models were based on alkali halide salts. However, the implication of an EDL for complex structure-making cations, such as Mg, Al, Fe, Zn, has been far less obvious. Though there exists a small number of studies exploring the effect of cations on the interfacial water, much attention has been devoted to anions. An exploration of structure-making cations offers a unique paradigm to the molecular picture at the air/water interface.

In their 1968 study, Jarvis and Scheiman revealed a nonlinear relationship of electrostatic potential difference and highly concentrated $MgCl_2$ solutions (Figure 1.1). In contrast to simpler

salts (NaCl, $NaNO_3$, Na_2SO_4), solutions of $MgCl_2$ and $MgNO_3$ appear to diverge significantly from a linear trend. While the authors acknowledge ion specific effects, no exclusive consideration was given to the role of cations at the time.[15,18] Only more recently, MD simulations of interfacial $MgCl_2$ solutions showed the disruptive influence of Mg^{2+} on water-water hydrogen bonds at higher concentrations compared to Na^+.[24] Unlike the electrostatic forces of Na^+ with water molecules (solvated ion), Mg^{2+} is held-tightly to six water molecules in its first hydration shell (metal aqua ion)[25]. A second hydration shell is merely six, or twelve, consecutive water molecules that are hydrogen bonded to the waters of the first solvation shell. Indeed, the second shell water experiences some electrostatic forces with the central metal cation[26]. Given the complexity, the $[Mg\ (H_2O)_6]^{2+}$ ion can be expected to affect the interfacial water-water hydrogen bonds at very high concentrations. Indeed, the MD simulations, in conjunction with VSFG and heterodyne SFG, reveal the presence of solvated ion pairs (SIPs) in aqueous $MgSO_4$ which influence the EDL in the interfacial water region.[24] The SIPS affect the orientation of the water dipole molecules which were detected by the phase sensitive HD-VSFG.

The complexities of the air/water interface must be explored via multiple techniques, both macroscopic and microscopic, to obtain a holistic molecular level understanding of ion interaction in the interfacial rearrangement of water. In this regard, constructing a suitable surface potential instrument is a justifiable venture for continued research on this frontier.

1.3 Objectives

This thesis sought to detail the design and construction of an ionizing method surface potential (SP) instrument. This instrument is validated by measuring the surface potentials and reporting on the trends that provide insight on the molecular level behavior of charged surfactants (SDS, CTAB) and salt solutions (NaCl, $MgCl_2$, $NaSO_4$, $MgSO_4$).

Chapter 2 ELECTRICAL PHENOMENA AT THE INTERFACE

2.1 Introduction

Charged particles tend to segregate at most interfaces in a direction normal to the phase boundary. This separation of charges may appear due to preferential adsorption of either positive or negative ions at the interface, adsorption and orientation of molecular dipoles, or via transfer of charge across the phase boundary. Intermolecular interactions at the liquid surface leads to a small net orientation of dipoles, which generates the corresponding dipole potential. Since the interface is complex, it is important to define the electrostatic potential of a phase.

2.2 Theory: Defining potentials at the interface

Surface potential is a term which means the change in electrical potential at the interphase between a medium and vacuum.[27] This change in electrical potential itself arises from a monolayer, or several layers of dipoles with degrees of orientation, and also from the preferential adsorption and desorption of ions in the EDL (Section 2.4).

The **surface potential (χ)** for a unit charge moving from vacuum into a medium is related to its **inner potential (φ)** and its **outer potential (ψ)**.

$$\varphi = \psi + \chi \tag{2.1}$$

This relationship is illustrated in Figure 2.1. The physical significance of these terms have been defined by Parsons[28].

φ is the total work required to move a unit charge from a point in the bulk of the vacuum to a point in the bulk of the medium. As per Equation 2.1, φ can be broken into two parts: ψ and χ. ψ is the work required to move a unit charge to a point "just outside the surface" as coined by

Bard and Faulkner[29]. “Just outside the surface” is an imaginary boundary where a unit charge experiences negligible interactive forces. Moving deeper towards the bulk of a medium, the unit charge experiences forces due to interactions with the dipoles of the medium. The work done experienced by the unit charge here is called χ.

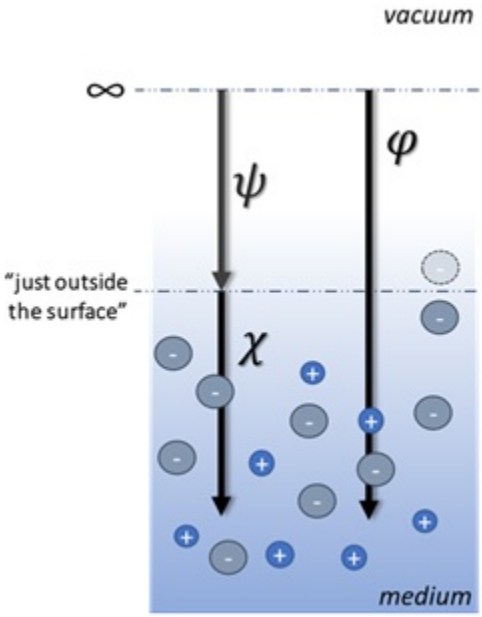

Figure 2.1 Relationship between the different potentials for a medium.

For a charged species, the **chemical potential ($\boldsymbol{\mu}$)** is modified as the effective chemical potential or **electrochemical potential ($\boldsymbol{\tilde{\mu}}$)** (also called the partial molar Gibbs energy) to account for the presence of electric potential in the region where these species exist. For species z_i in phase β, the associated electric potential is φ^{β}. Therefore,

$$\tilde{\mu}_i^{\beta} = \mu_i^{\beta} + z_i F \varphi^{\beta} \qquad (2.2)$$

When phase β is in contact with phase α, the $\tilde{\mu}$ of each phase is in thermodynamic equilibrium.

$$\tilde{\mu}_i^{\alpha} = \tilde{\mu}_i^{\beta} \tag{2.3}$$

By combining 2.2 and 2.3, the **electric potential difference ($\Delta^{\alpha\beta}\varphi$)** between the two phases can be related as follows:

$$\mu_i^{\beta} + z_i F \varphi^{\beta} = \mu_i^{\alpha} + z_i F \varphi^{\alpha}$$

$$\varphi^{\beta} - \varphi^{\alpha} = \frac{\mu_i^{\alpha} - \mu_i^{\beta}}{z_i F}$$

$$\Delta^{\alpha\beta}\varphi = \varphi^{\beta} - \varphi^{\alpha} = \frac{\mu_i^{\alpha} - \mu_i^{\beta}}{z_i F} \tag{2.4}$$

$\Delta^{\alpha\beta}\varphi$ has been termed the Galvani potential difference between two specific points within the bulk phases of α and β.[30] Based on Equation 2.4, it is apparent that $\Delta^{\alpha\beta}\varphi$ is depends solely on the change in μ between the two phases. Note that it is not possible to measure $\Delta^{\alpha\beta}\varphi$ between two phases of different chemical compositions. Despite the differences in chemical composition, $\Delta^{\alpha\beta}\varphi$ can be measured in multiphase systems where the $\tilde{\mu}$ of phases are known to be theoretically equal. This is elaborated in Section 3.2.1.

For two condensed phases with the same chemical composition, the ψ of the two phases are equal when there is no electric field in the space between them. For example, two solid phases[31] or a solid and liquid[14,27]. Thus,

$$\psi^{\alpha} = \psi^{\beta}$$

$$\Delta^{\alpha\beta}\psi = \psi^{\beta} - \psi^{\alpha} = 0 \tag{2.5}$$

If the χ of one phase changes, $\Delta\psi$ equal zero (ψ remains constant). Given the relationship of these potentials (Equation 2.1), $\Delta^{\alpha\beta}\psi = 0$ means $\Delta^{\alpha\beta}\varphi$ equals $\Delta^{\alpha\beta}\chi$:

$$\Delta^{\alpha\beta}\varphi = \Delta^{\alpha\beta}\psi + \Delta^{\alpha\beta}\chi$$

$$\Delta^{\alpha\beta}\varphi = \Delta^{\alpha\beta}\chi \tag{2.6}$$

2.3 Relating surface potential to the structure of interfaces

Changes in surface potential provide insight on the distribution and structure of ions and molecules at the surface. χ itself is derived from oriented dipoles across the surface and the preferential adsorption and desorption of ions in EDL.

$$\chi = \chi_{molecular\ dipoles} + \chi_{EDL} \tag{2.7}$$

Thus, contributions to the χ arise from polarized atoms or molecules and from the partition of ions based on charge in a direction normal to the surface. At any interface, both the molecular dipole potentials and the EDL contribute to the total potential drop across an interface. The influence of χ for one species cannot be measured independently of the other.

2.3.1 Molecular dipoles

If we consider an array of molecular dipoles at the surface, the surface dipole can be equated to two plates of a charged parallel-plate capacitor.[31] The electric field between the parallel plates is the ratio of charge density along the plate surface to the permittivity of the medium. The distance between the two plates of such a capacitor can be regarded as the distance between two poles of a dipole being measured normal to the surface. With application of electrostatic theory, the χ can be considered as,

$$\chi_{\,molecular\ dipoles} = \frac{N\mu_{\perp}}{\epsilon_0} \tag{2.8}$$

where N is the number of diploes per unit area of surface, $\mu_{\perp}$ is the normal component of each dipole, and ϵ_0 is the permittivity of free space. For Langmuir monolayers, often made up of amphiphilic molecules, the surface dipole moment μ is represented by a more complex quantity consisting of several dipole components corresponding to the different dipolar regions within a single molecule.[32,33,34]

2.3.2 The electric double layer

Knowledge of ion distribution near the phase boundary is necessary because of the electric field produced by a net charge of ions from the electrolyte. Ion are either repelled or attracted to the interface. Random thermal motion of ions also take place. Since the interface is charged, it follows that the fluid adjacent must be charged to balance the surface charge. This makes the surface and solution electrically neutral. The charged area at the surface is the Stern layer, whereas the free moving ions governed by electrostatic and thermal forces is the diffuse layer. Together, they make the electric double layer (Figure 2.2).

In terms of ion distribution, the Stern layer is where the potential drop is linear due to the adsorption of ions at the surface of the solid itself. The next layer is termed the diffuse layer where the potential drop is more exponential (per Boltzmann decay). Together, these layers provide a descriptive model of the drop-in potential within the liquid phase itself. While the Stern layer is easily defined based on the position of ions, the diffuse layer is more random. The position of each ion is relatively unknown and so the distribution is described using the Poisson-Boltzmann equation.

With respect to the **charge density of a point charge in space** ($\boldsymbol{\rho}$) and $\Delta\varphi$, the net charge per unit volume of this point is described by the Poisson equation:

$$\nabla^2(\Delta\varphi) = -\frac{\rho}{\epsilon_r\epsilon_0} \tag{2.9}$$

where ϵ_r is the dielectric constant of the solution. Ions in the diffuse region must be in equilibrium, the force electrochemical must be zero:

$$\mathrm{kT}\nabla\ln(N_\mathrm{i}) + \mathrm{z}_i e\nabla(\Delta\varphi) = 0 \tag{2.10}$$

where $N_\mathrm{i} = N_A c_i$. This gives the Boltzmann distribution equation:

$$N_\mathrm{i} = N_{0,i}\exp^{\left[\frac{-\mathrm{z}_i e\Delta\varphi}{kT}\right]} \tag{2.11}$$

where N_i and $N_{0,\mathrm{i}}$ are respectively the numbers of ions per unit volume. Since the free-charge density equals charges arising from ionic species,

$$\rho = \sum_\mathrm{i} -\mathrm{z}_i e N_i \tag{2.12}$$

Thus, from combining these expressions the *Poisson-Boltzmann equation* is obtained*:*

$$\Delta\varphi = -\frac{1}{\epsilon_r\epsilon_0}\sum_i z_i e N_{0,i}\exp^{\left[\frac{-z_\mathrm{i}\mathrm{e}\Delta\varphi}{kT}\right]} \tag{2.13}$$

Equation 2.19 forms the basis of Gouy-Chapman-Grahame model of diffuse layer adjacent to a charged surface.[20] This is further explored in Section 2.5.

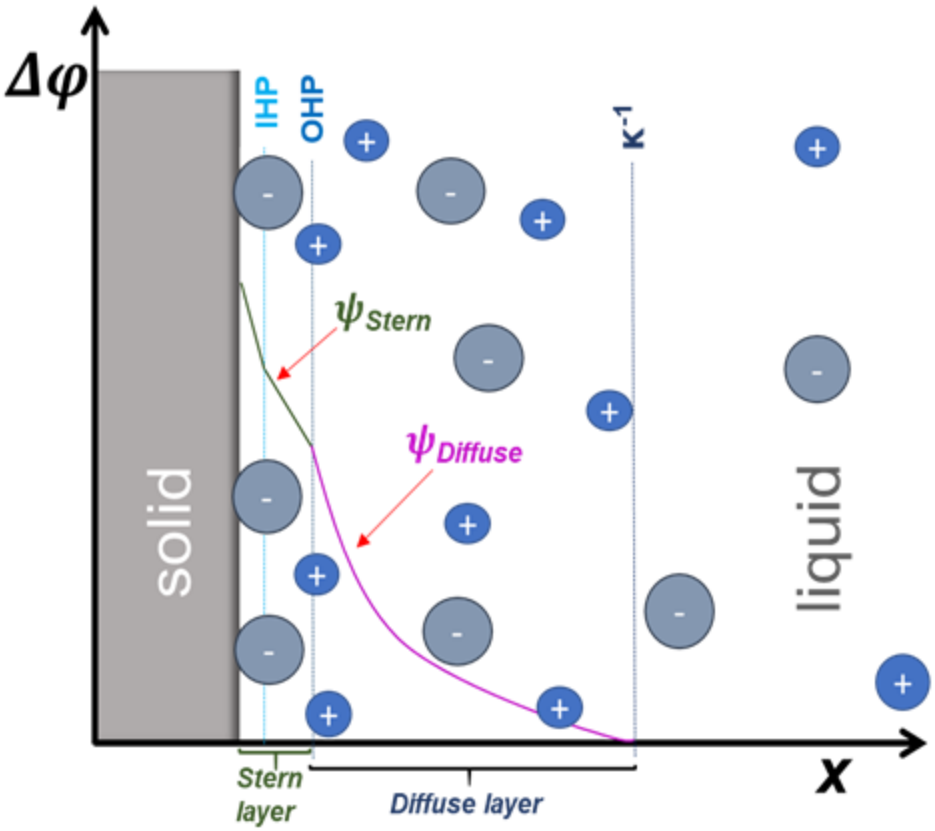

Figure 2.2 Illustration of the electric double layer capacitor model at the solid-liquid interface. The Stern layer is a compact region of adsorbed ions (inner Helmholtz plane, IHP) and non-specifically adsorbed ions (outer Helmholtz plane, OHP). The boundary of the electric double layer and bulk regions is determined by the Debye length (κ^{-1}).

2.3.3 Application to aqueous electrolyte surface

The relevance of surface potential for the air/water interface is understanding how χ originates from the interplay of molecular dipoles and ions in the EDL. For charged molecular groups on the water subphase, the Gouy−Chapman-Grahame EDL model is widely utilized to describe the impact of these moieties on the composition of adjacent layers of solution and the concentration of electrolyte ions that counter the surface charge.[34,35] The interaction of water molecules, solvated ions, and charged molecules occurs through hydrogen bonding, electrostatic interactions, and van der Waals forces. This interfacial region is called the "bonded interface layer (BIL)" network.[36,37] Adjacent to this region is the diffuse layer where the water subphase has a more bulk-like hydrogen bonding structure. These waters are influenced by long-range effects of surface charges and screening ions.[29,38,39]

For a pure electrolyte solution, however, the χ arises from the molecular dipole arrangement of water molecules and the preferential adsorption or desorption of ions.[15,27] Though density profiles of ions at the air/water interface show the precise selectivity of ions for the water surface, the model is limited by assuming the interface is an infinitesimal plane that divides air and water. Guggenheim[40] showed that the interface of a real system must have some thickness. Therefore, unlike the solid-liquid interface or charged air/water interface, the χ profile might be expected to be continuously non-linear based on Boltzmann-like distribution of ions within the layers of interfacial waters and the forced and/or inherent orientation of interfacial waters. Additionally, the χ profile of the air/water interface will be largely dependent on the type

of ions[23], number of ions at the interface (due to the Debye length)[27], and the dipolar and quadrupolar contribution of water[41].

$$\chi_{ionic\ interface} = \chi_{cations} + \chi_{anions} + \chi_{water} \tag{2.14}$$

To isolate the χ contribution of one species over the other by either modelling or measuring surface potentials is not a trivial matter.

2.4 Relevance of Debye length for electrolytes

The range of electrostatic effects by the ions in the diffuse layer is specified by the **Debye length**($\boldsymbol{\kappa^{-1}}$). For the air/water interface, Randles[27] regards the region through which the interplay of ions and water dipoles contribute to surface potential to be equivalent with the κ^{-1}. Figure 2.3 relates the thickness of this layer with concentration and type of ions in the solution. Higher concentrations and higher ion valences are more effective at screening charge.

Debye-Hückel parameter (κ) is related to $\Delta\varphi$ by a derived form of the Poisson-Boltzmann equation (2.13) and can be rewritten as:

$$\frac{\partial^2 \Delta\varphi}{\partial x^2} = \kappa^2 \Delta\varphi \tag{2.15}$$

where κ is defined as

$$\kappa = \sqrt{\frac{e^2}{\epsilon\epsilon_0 kT} \sum_i z_i^2 N_i} \tag{2.16}$$

To predict a profile of $\Delta\varphi$ with increasing distance x into the bulk of the solution, the boundaries of the diffuse layer must be applied. As $x \to \infty$, $\Delta\varphi \to 0$, the

$$\Delta\varphi = \Delta\varphi_o e^{-\kappa x} \tag{2.17}$$

The potential decreases exponentially. The Debye length is simply the inverse of (2.16), where $N_A c_i$ in mol/dm^3:

$$\kappa^{-1} = \left[\frac{2e^2}{\epsilon_r \epsilon_0 kT} \sum_i z_i^2 N_A c_i\right]^{\frac{1}{2}} \tag{2.18}$$

Independent of surface charge or potential, the magnitude of κ^{-1} depends on the properties of the solution. Figure 2.6 summarizes the effect of electrolyte on Debye length. With increasing concentration and valence of the electrolytes, κ^{-1} decreases to a large extent. The effect of electrolytes in reducing the κ^{-1} varies by a factor of 4 for between 3:1 and 1:1 electrolyte solution (Figure 2.3). The effects between a 1:2 and 2:1 electrolyte solutions are relatively similar.

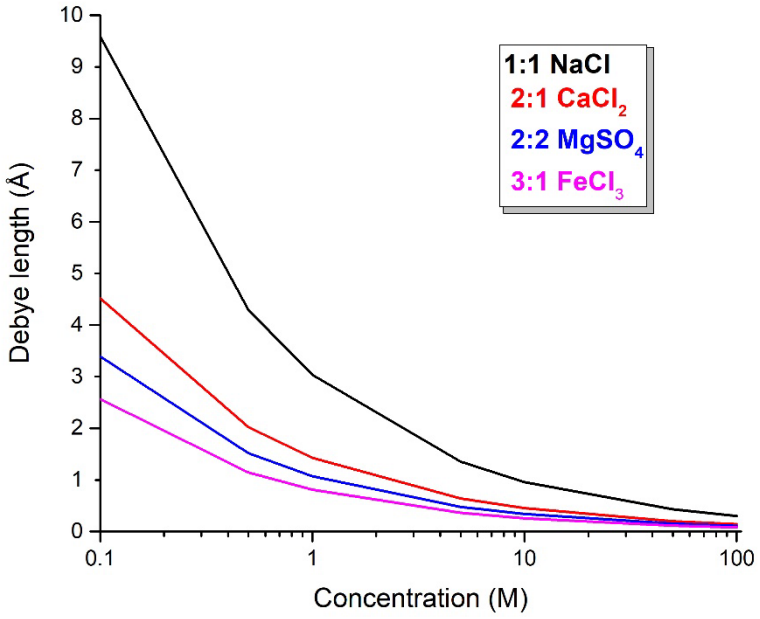

Figure 2.3 Variation of Debye length with concentration of different electrolytes.

Table 2.1 Thickness of the Diffuse Layer. [a]Concentration (mol/dm^3) [b]For electrolytes at 25°C in water.

Concentration[a] (M)	**Debye length[b] κ^{-1}(Å)**			
	1:1	**2:1**	**2:2**	**3:1**
3	1.8	0.8	0.6	0.5
1	3.0	1.4	1.1	0.8
10^{-1}	9.6	4.5	3.4	2.6
10^{-2}	30.3	14.3	10.7	8.1
10^{-3}	96	45	34	26
10^{-4}	303	142	107	81

2.5 Charged groups at the surface

Amphiphilic molecules at the air/water interface impart a surface charge on the water surface. If a number of these molecules are present on the surface, how does **surface charge (σ)** and φ relate? The Grahame equation relates the surface charge density of ions at the surface to their surface potential based on Gouy-Chapman theory.[42]

As the double layer is electrically neutral, the σ must be balanced by the charges in solution. Taking ρ in directon x towards the surface,

$$\sigma = -\int_0^\infty \rho(x)\, dx \tag{2.19}$$

Combined with (2.19) and integrated to give,

$$\sigma = \sqrt{\left(-2\epsilon_r\epsilon_0 kT \sum_i N_i \left\{\exp^{\frac{-z_i e^- \varphi_\infty - \varphi_x}{kT}} - 1\right\}\right)} \tag{2.20}$$

Equation (2.20) is relatively inconvenient to use. A reduced but equivalent form is more commonly used and otherwise known as the *Grahame equation* (2.21). This form is simplified for a system containing only one symmetrical electrolyte (2:1 or 1:2) where $N_i = N_A c_i$ in mol/m^3 and $z_{\mp} = z$:

$$\sigma = \sqrt{(8kT\epsilon_r\epsilon_0 N_A c_i)}\,sinh\left[\frac{-z_i e}{2kT}\Delta\varphi\right] \tag{2.21}$$

The calculated relationship between surface potential and surface charge for a 1:1 salt is shown in Figure 2.4. The surface potential is reduced with increase in surface charge. The more concentrated, the lesser the potential with increasing charge.

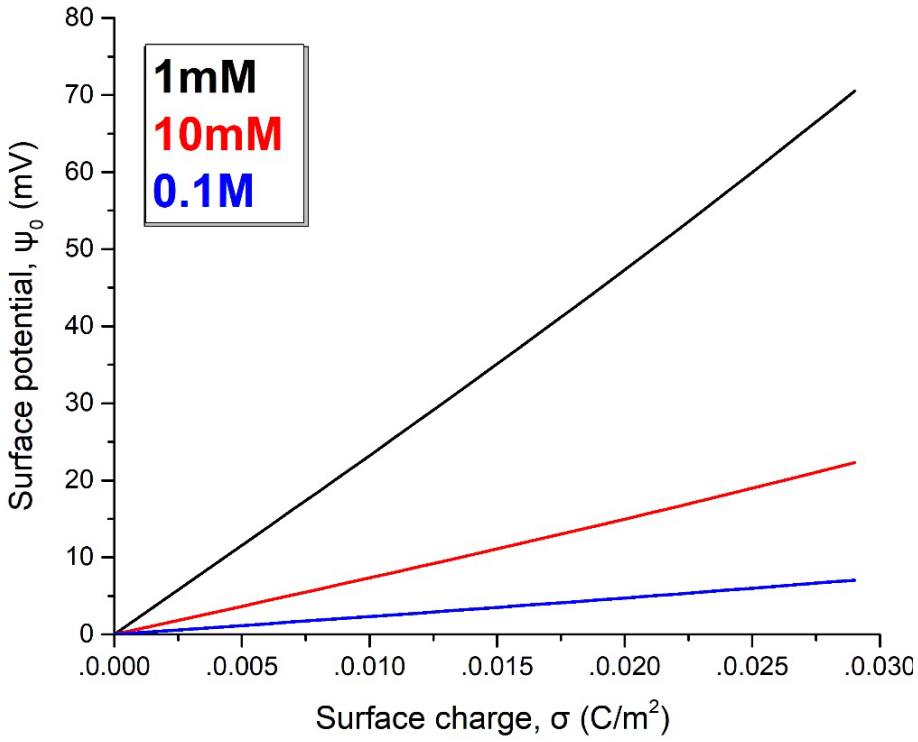

Figure 2.4 Hypothesized surface potentials versus surface charge for 1:1 salt at different concentrations using the Grahame equation. The temperature was assumed to be 25°C.

Chapter 3 SURFACE POTENTIAL

3.1 Introduction

This chapter summarizes the theory, design, and fabrication of an ionizing method based surface potential (SP) instrument. This variation of the ionizing electrode methods was first proposed by Guyot[43] and used by several others[17,44,45]. Section 3.2 provides a simplified theory of surface potential measurement, followed by a section on interpretation of measured potentials. Details on instrument configuration and parameters are also outlined following Section 3.2.

3.2 Measuring potentials across the air/water interface

While there are several ways of measuring E, the two commonly used techniques are the vibrating-plate[46,47,48] and the ionizing method[49]. For the first, a plate vibrates vertically with respect to the surface of the water. The mechanical movement induces change in the air gap leads an alternating current to flow in the external circuit, whereby magnitude of current is proportional to the potential difference. In the second technique, a radioactive probe ionizes the gap between air and water. The gaseous ions produced carry current between the two phases which is detected by a galvanometer (a sensitive electrometer in voltage mode). Comparatively, the ionizing method is a direct current method of measuring E versus the vibrating plate which is an alternating current method.

Despite their differences, both techniques have one principal in common: measuring ΔV requires two electrodes: one placed in the bulk of the aqueous subphase and the other suspended above the solution in air. The theory of this is explained in the following section and presented as a simplified version of the argument provided by Parsons[50].

3.2.1 Theory: Measuring $\Delta\chi$

In principal, $\Delta\chi$ across the liquid-gas interface is measured between two electrodes: one placed in the bulk of the aqueous subphase and the other suspended above the solution in air. This system can be illustrated in the following schematic, where the vertical bar denotes a phase boundary:

Air (phase α) | Ionizing probe (Ip) | Platinum gauze (Pt) | Electrolytic solution (phase β)

For clarification, the phases of the electrodes must be considered to measure $\Delta\chi$.

Consider the two metal electrodes, Ip and Pt, connected in series through a potentiometer measuring potential E in a zero-electric field environment. Pt is placed in solution (phase β) and Ip is suspended in the air (phase α). The following relationships hold when Ip and Pt are considered to have their own phase.

As there is no current flowing across the gap between Ip and the surface of β, their ψ must equal each other as per Equation 2.5.

$$\Delta^{\mathrm{Ip}\beta}\psi = \psi^{\mathrm{Ip}} - \psi^{\beta} = 0 \tag{3.1}$$

Therefore, $\Delta^{\mathrm{Ip}\beta}\varphi$ will directly equal $\Delta^{\mathrm{Ip}\beta}\chi$.

Since Pt is in contact with phase β, the $\tilde{\mu}$ of their electrons are equal,

$$\tilde{\mu}_e^{\beta} = \tilde{\mu}_e^{\mathrm{Pt}} \tag{3.2}$$

The $\tilde{\mu}$ of Ip and Pt can be related by potential ϕ as they are connected through the potentiometer,

$$\begin{aligned} \phi z_e F &= \tilde{\mu}_e^{\mathrm{Ip}} - \tilde{\mu}_e^{\mathrm{Pt}} \\ &= \tilde{\mu}_e^{\mathrm{Ip}} - \tilde{\mu}_e^{\beta} \end{aligned} \tag{3.3}$$

where $z_e F$ relates to the quantity charge per mole of electrons between the electrodes.

Applying 2.2 to 3.3, $\tilde{\mu}_e^{\mathrm{Ip}}$ and $\tilde{\mu}_e^{\beta}$ is expanded to include their respective μ and φ,

$$\tilde{\mu}_e^{\mathrm{Ip}} = \mu_e^{\mathrm{Ip}} - z_e F\varphi^{\mathrm{Ip}}$$

$$\tilde{\mu}_e^{\beta} = \mu_e^{\beta} - z_e F\varphi^{\beta}$$

Thus,

$$\tilde{\mu}_e^{\mathrm{Ip}} - \tilde{\mu}_e^{\beta} = \mu_e^{\mathrm{Ip}} - \mu_e^{\beta} - z_e F(\varphi^{\mathrm{Ip}} - \varphi^{\beta}) \tag{3.4}$$

With the ionization of the air gap between Ip and Pt, an electric field is created which causes their respective $\tilde{\mu}$ to equal, i.e., $\tilde{\mu}_e^{\mathrm{Ip}} = \tilde{\mu}_e^{\beta}$. Equation 3.4 simplifies to:

$$\Delta^{\mathrm{Ip}\beta}\varphi = \varphi^{\mathrm{Ip}} - \varphi^{\beta} = \frac{\mu_e^{\beta} - \mu_e^{\mathrm{Ip}}}{z_e F} \tag{3.5}$$

Combining Equations 3.3 and 3.4,

$$\phi_{\beta} = \Delta^{\mathrm{Ip},\beta}\varphi \tag{3.6}$$

where $\boldsymbol{\phi_{\beta}}$ represents the **measured inner potential difference in phase $\boldsymbol{\beta}$**. Analogously, ϕ_{α} in phase α is,

$$\phi_{\alpha} = \Delta^{\mathrm{Ip},\alpha}\varphi = \varphi^{\mathrm{Ip}} - \varphi^{\alpha} \tag{3.7}$$

The measured E by the potentiometer is equivalent to ϕ for α and β,

$$\begin{aligned} E &= \Delta^{\alpha,\beta}\phi = \phi_{\alpha} - \phi_{\beta} \\ &= (\varphi^{\mathrm{Ip}} - \varphi^{\alpha}) - (\varphi^{\mathrm{Ip}} - \varphi^{\beta}) \\ &= \varphi^{\mathrm{Ip}} - \varphi^{\alpha} - \varphi^{\mathrm{Ip}} + \varphi^{\beta} \\ &= \varphi^{\beta} - \varphi^{\alpha} \end{aligned} \tag{3.8}$$

Using the relationship in Equation 2.6, the **measured surface potential** ($\boldsymbol{E}$) directly relates to the change in surface potential.

$$E = \chi^{\beta} - \chi^{\alpha} \tag{3.9}$$

With respect to the air/water interface, the χ^{α} of air (phase α) can also be assumed to be constant as there are almost no ions or particles that causes potential changes in that in that phase. Therefore, E relates directly to χ^{β} of phase β.

The experimental practice of reporting surface potential E varies from one study to another. Often, studies report surface potentials relative to a pure subphase as ΔV. For example, ΔV measurements of monolayers are reported as the difference of the measured E for a surfactant and the bare surface:

$$\Delta V = E_{monolayer} - E_{bare\ surface} \tag{3.10}$$

The purpose for this is to determine the surface potential associated merely with the monolayers. In studies with inorganic electrolytes, the ΔV is not as useful for analysis as a large contribution to E comes from the dipolar and quadrupolar contributions of water.[51] This is further discussed in the next section.

3.2.3 Interpreting sign and magnitude of surface potentials

As described in previous sections, interpreting E is assessed in respect to pure water or a bare surface. In terms of magnitude, measuring E is directly related to the effect of the molecular dipoles and the EDL. Assuming a salt-only solution is being measured, measured E relates to the influence of ions on the molecular dipole and quadrupole components of water (Equation 2.14).

For salt solutions, the ionic charge is shaped by its interaction with the asymmetric hydrogen-bonding network of surface water molecules.[52] Ions have been shown to alter the hydrogen-bonding arrangement of interfacial water.[53] In what is known as the flip-flop model of

interfacial water molecules, the dipoles of water orient either towards or away from the surface depending on interaction with charged distributed species at the interface.[54] For example, a negatively charged substance on the surface of water will impart a negative charge on the surface. Water molecules will, therefore, orient with their hydrogens pointed towards the interface. For a positively charged interface, the water molecules will orient oxygen up towards the interface. This effect has been experimentally demonstrated by HD-VSFG.[55] This effect has since been used by Randles[15] to interpret surface potential changes for preferential adsorption and desorption of ions in electrolyte solutions.

3.2 SP Design and Construction

3.2.1 Equivalent circuit

As described earlier, the circuit schematic in Figure 3.1 shows how measuring the air/water interface is akin to a complex cell.[56] For this setup, the **voltage source (V_S)** is the air/water sample and the **voltage measured (observed) (V_M)** is the measured E with the potentiometer. The **air/water gap** has an extremely large **resistance (R_S)** because air is a good insulator.[57] Ip and Pt are connected in series through the potentiometer. The potentiometer itself has a large **internal resistor (R_{IN})**. Applying Ohm's law to the circuit gives us the following relationship:

$$\frac{V_M}{V_S} = \frac{R_{IN}}{R_S + R_{IN}} \tag{3.11}$$

As per Equation 3.7, the accuracy of V_S depends on the ratio of R_{IN} to R_S. Supposing R_{IN} is ~10^{14} and R_S is ~10^{11}, there is an approximately 1% difference in V_M. Equation 3.11 can be used to correct differences between V_M and V_S.

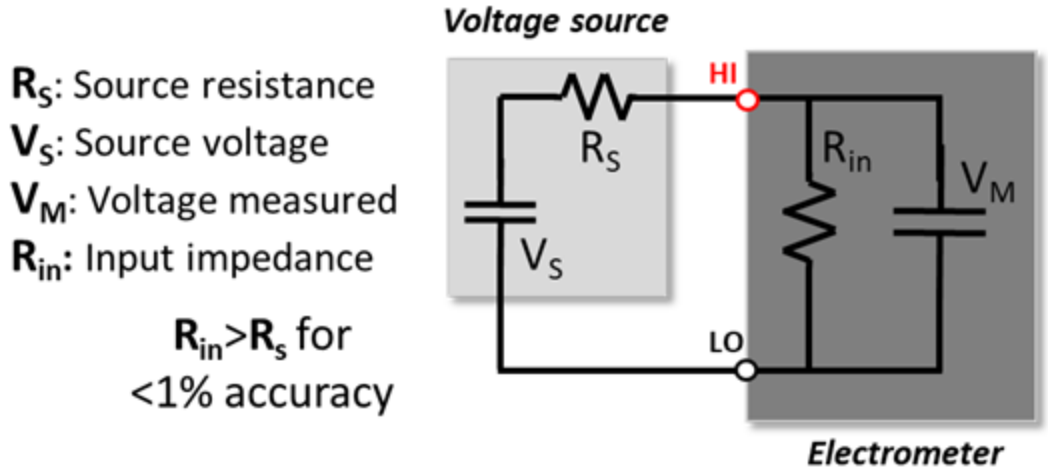

Figure 3.1 Equivalent circuit diagram of SP instrument

3.2.2 Parts

The ionization source consists of an americium-gold matrix incorporated as a rolled foil with an aluminum backing with a 9.5mm active diameter purchased from Eckert & Ziegler Isotope Products (Valencia, CA). A copper contact piece was machined to establish a good electrical connection with the source and serve as connection to the triaxial cable. The platinum gauze electrode (25 x 35mm) was purchased from BioLogic Science Instruments (Knoxville, TN). A Keithley 6517B Electrometer/High Resistance Meter with humidity and temperature probe attachments were purchased from Tektronix (Beaverton, OR). The electrometer was interfaced with a computer using the LabView program purchased from National Instruments (Austin, TX). A copper Faraday enclosure (Ø0.25 mm wire, 1.4 mm spacing) was purchased from Thorlabs (Newton, NJ). The enclosure houses a heavily damped and vibrational isolated

breadboard inside. An additional Plexiglas enclosure was used to house the setup inside the Faraday enclosure to minimize air drifts during measurement.

3.2.3 Design

1. Scheme

The SP is constructed with an ionization source and inert counter electrode coupled to a high resistance electrometer (Figure 3.2). The setup is placed inside a Plexiglas box inside a Faraday cage. A nitrogen gas purge is used to help reduce the relative humidity surrounding the setup close to a constant 25%. The electrometer connections are illustrated based on the colors of a low noise triaxial cable with a BNC connector that connects to the back panel of this model electrometer. The red line refers to connection of Ip to the input high (positive) and the black line

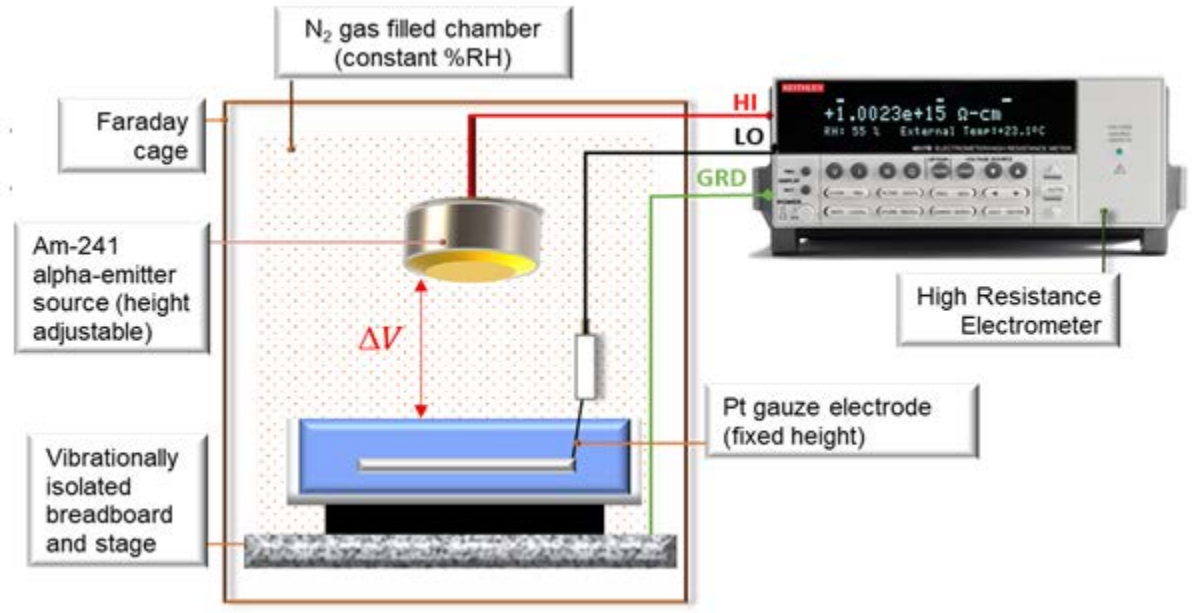

Figure 3.2 Scheme of SP instrument used in these experiments.

connects Pt to the common (negative). Green is the chassis ground wire connected via an alligator clip connection to a fixed screw on the breadboard. Not shown in the scheme below is the laser displacement sensor used to determine the height of solution from one experiment to the next.

2. Electrodes

Air is a poor conductor of electricity as gaseous molecules are not in continuous contact with each other to provide an electrical pathway. Electrical contact with the subphase is established through an ionized air gap. The radioactive element of the Ip used in these studies is Americium-241 (activity: 20μCi (740kBq), alpha energy: 4.7MeV). Because Ip acts as both an ionization source and a working electrode, one might expect it to have a reference potential. However, the undefined nature of the radioactive probe means this potential is unknown.[18] The Ip is mounted on a micrometer stage allowing the vertical height to be adjusted above the subphase. Since this application of SP involves electrolytes, Pt is the most suitable counter electrode. Pt is ideal due to its low resistivity and chemical inertness, making it less susceptible to corrosion.[58] A triaxial cable connection of these electrodes to the Keithley 6517B is illustrated in Figure 3.2.

3. Electrometer

The limit of sensitivity for any measurement is determined by noise. Voltage noise is proportional to the square root of source resistance, noise bandwidth, and absolute temperature of the system. For SP, the high source resistance (>1GΩ) is the limiting factor in sensitivity of V_M. While measuring 1μV is possible at 1mΩ resistance, noise prohibits any possibility of

measuring the same voltage at 1TΩ (Figure 3.3). Even measuring 1μV at somewhere near 1GΩ is nearly impossible for an ordinary digital multimeter. Digital multimeters also have a large enough input bias current (or offset current) that inhibits accurate measurement of voltage at higher resistances.[59]

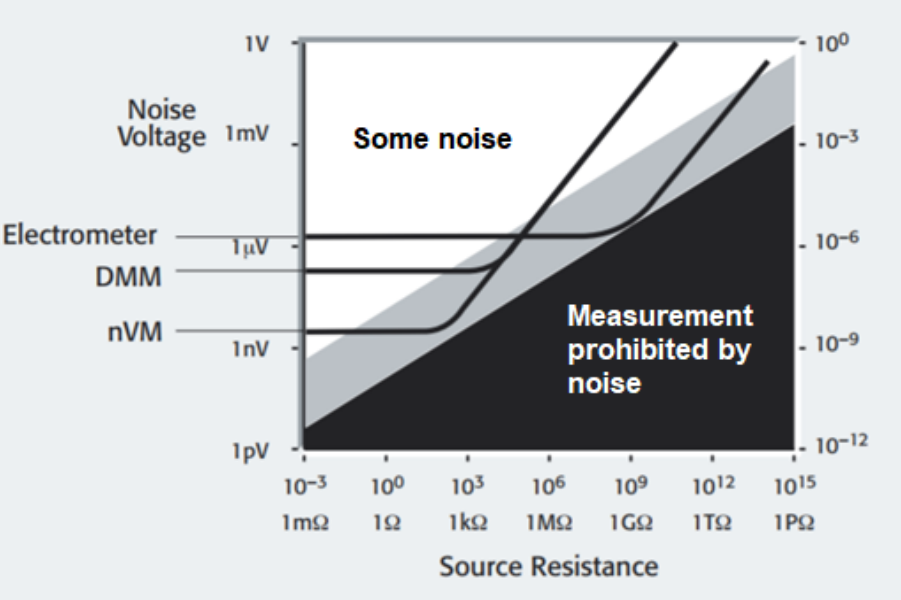

Figure 3.3 A comparison of devices (electrometer, digital multimeter (DMM), nanovolt meter (nVM) used to accurately measure low-level signals in high resistance regimes. Between the two noise regions is where an instrument can distinguish noise from signal (greyed area). Figure taken from Low Level Measurements Handbook, ed.7 published by Keithley/Tektronix.

Due to its capability in accurately measuring response in regions close to 1GΩ, an electrometer is the ideal device to accurately measure low level voltages. The fundamental working of an electrometer voltmeter is the extremely high input resistance (200TΩ) and the input bias current is less than 3fA. These characteristics permit electrometers to make accurate measurements without introducing a large bias into the circuit. The electrometer sensitivity used in the SP instrument is ±0.001 mV.

4. Laser displacement sensor

An LK-H057 laser displacement sensor was purchased from Keyence Corporation (Itasca, Illinois). The sensitivity of this instrument was ±0.001 cm for a laser beam reflecting off a diffuse surface. The laser head is mounted on the same stage as Ip. The purpose of the sensor is to determine the height of subphase relative to Ip. A constant height is important to decrease errors of V_M due to height differences of subphase between samples.

5. Faraday cage

A Faraday cage helps minimize influence of external electromagnetic waves on the SP. Waves longer than the 1.4mm spacing taut copper mesh are blocked. The breadboard mounted inside the cage sits on a rubber padded vibration-isolators. This arrangement prevents interference of the cage with the breadboard itself. The effectiveness of the cage is shown to be around 10MHz (Figure 3.4). Due to the relatively large surface of the breadboard and the tendency of its metal surface to hold static charges, a grounding strap is used to connect the breadboard to the Faraday cage. An exterior ground strap is used to ground the enclosure to a metal pipe of the building. Using a Fluke 115 Digital Multimeter (DMM), grounding

effectiveness is tested by measuring potential difference from a known ground to the different points on the Faraday cage.

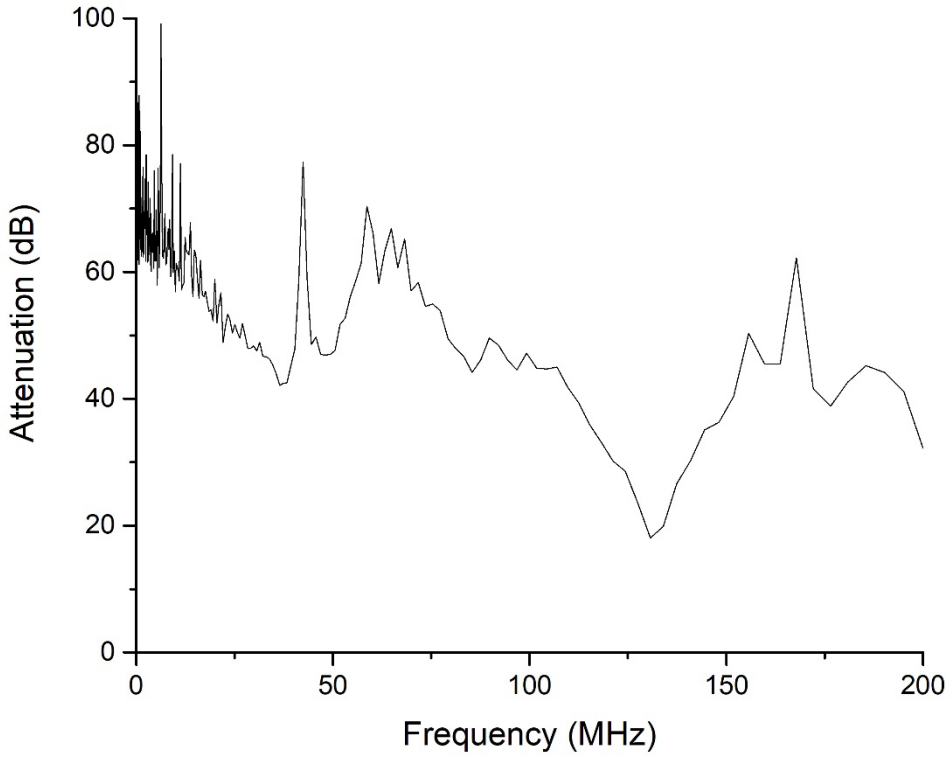

Figure 3.4 Graph of Faraday cage shielding effectiveness shows shielding is most effective around 10-15 MHz (~60 dB). Data courtesy of Thorlabs and used with permission.

3.3 Validating electrometer response to experimental setup

Several configurations were tried, tested, and ultimately not workable due to unsteady reading, noise, or bad design. The current SP setup is a relatively good configuration as it allows control for the height of the ionizing probe with respect to the solution. Initially, there were experimental problems due to the other factors such as noise or stray current for which grounding, shielding, and experimental procedures effectively resolved these issues. The following subsection outlines factors that may affect measurement.

3.3.1 Grounding and shielding

The purpose of grounding is to remove capacitive charge between metals by redirecting electrical charges away from the setup to minimize interference. Typically, good grounding is seen in building structures as proper large-scale equipment performance is dependent on isolation.[60] However, the same building might be the source of interference for electrical measurements, particularly voltage detection. Therefore, a well-designed Faraday cage is central to shielding an electrical setup from external interferences (Section 3.2.3). In conjunction with each shielding, an effective electrical ground eliminates buildup of electrostatic charge. For this setup, several grounding tests were tried until noise in the signals dropped below 1mV (Figure 4.1).

There is a total of three grounding connections which were effective in reducing noise in the system. The first connection was to ground the immediate area surrounding the electrodes. This was done by connection of the vibrational isolated breadboard to the Faraday cage itself. A second connection was made between the chassis ground of the electrometer with the metal

breadboard. The chassis ground of the electrometer leads to the earth ground. The chassis ground acts as a point that can be considered to have zero voltage. With these two connections in place, the internal metal fixtures such as the humidity and temperature probes, and the shielded mounts for the electrodes were all shown to have constant voltage (zero) with the grounded breadboard. The third connection was established from the outside of the Faraday to a metal fixture in the laboratory. While this might not have had much of an effect on the settling of electrometer reading, it eliminates all static charges on the outside of the cage itself.

3.3.2 Height of the ionizing probe

Ionization in the air above the water must be concentrated in the gap between the electrode in the air and water surface to provide sufficient conductivity and help reduce electrical leakage to other electrical surfaces.[61] Of the several sources available for ionization, such as X-rays or β rays, radiation from α-particles is preferred as they are intense and last only a few centimeters. Comparing two popular ionization sources, Po-210 ($t_{0.5}$ = 24,000 years and Am-241 ($t_{0.5}$ = 458 years), both produce weaker γ-rays along with the required α-particles and minimized shielding measures.[62] Foulkes[57] showed how α-particles with 5.5 MeV energy emitted into air ionize the air, creating ion pairs, 4 cm from the source. A similar calculation of the ionization by the Ip is shown in Appendix 1.

To understand the effect of ionization on the resistivity of the air/water gap, the height of Ip was varied with respect to the subphase of 1.5m $MgCl_2$. Beginning with 0.9 cm above the subphase, Ip was moved at 0.5 cm increments towards the subphase. V_M was found to be at a lower magnitude with the probe closest to the subphase. By applying a constant 40V to the

electrodes, the resistance of the setup was measured as well. The resistivity was calculated and shown in Figure 3.5. As mentioned earlier, the air/water gap is akin to an insulator. This insulator effect is obvious with the extremely high measured resistances. Figure 3.5 shows the dependence of this resistance with the height of Ip relative to subphase. For measurement purposes, the constancy of Ip height must, therefore, be maintained for consistent V_M from the subphase.

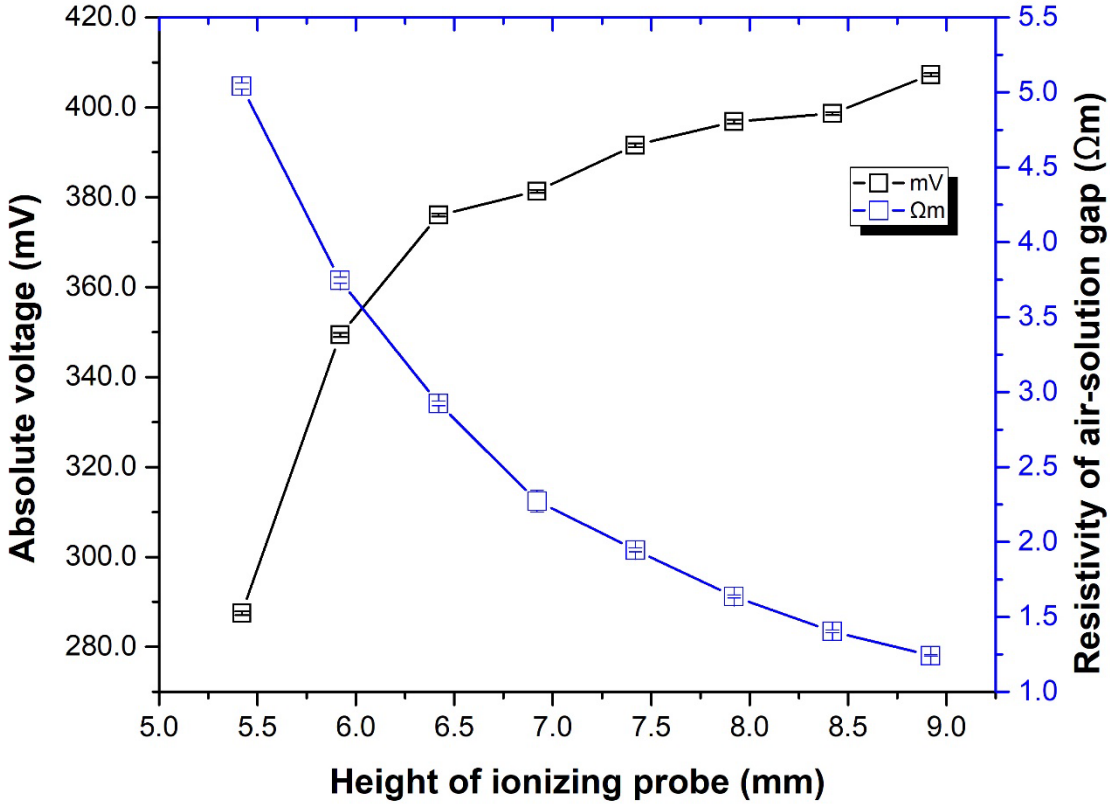

Figure 3.5 Plot of the distance of probe from surface of solution versus absolute voltage measured (black) and resistivity of the air-solution gap (blue).

3.3.3 Noise

Signal noise is highly dependent on the source itself. Thus, a good response produces a source V_S noise less than 1 mV which is within the 1% accuracy range of V_M. As mentioned earlier, the sensitivity of the Keithley 6517B is ±0.001 mV. For this setup, several sources of experimental noise are notable and summarized in the table below (Table 3.1). For reference, the shape of a typical signal measured is shown in Figure 4.1.

Table 3.1 Summary of the sources of noise based on signal response.

Signal Response	Reason
Good, i.e. <1 mV deviation over non-drift range	Proper grounding and setup. Proper experimental method in practice.
Total noise	Faraday cage/Plexiglass enclosure not completely shut. Triaxial cable not attached to electrometer. Ionizing probe is in contact with subphase.
Long term noise	Dirty surface or ionizing probe is in contact with the subphase.
Short term noise, possibly leading to drift	Setup has been bumped.
Drift (slanting shape)	Electrodes loosely attached. Dirty surface.
Sudden jump in signal observed	Ionizing probe is in contact with subphase.
Large difference (>50-100mV) observed from one set of experiments to another	Ionizing probe has residual amounts of aqueous subphase on its surface. The probe needs to be dried completely before use.

Chapter 4 EXPERIMENTAL METHODS

4.1 Chemicals

ReagentPlus®(≥98.5%, GC) SDS and CTAB (≥98%) as solid flakes were purchased from Sigma Aldrich and used without further purification. ACS grade (purity ≥99%) salts were purchased from Fisher Scientific: NaCl, Na_2SO_4, $MgCl_2$, $MgSO_4$. Ultrapure deionized water with a resistivity of 18.2 MΩ·cm and pH of 5.6 was obtained from a *Milli-Q*® Advantage *A10* (MilliporeSigma). All glassware and Teflon containers used primarily for salt solutions were treated with a concentrated 3:1 mixture of sulfuric acid and ammonium peroxydisulfate to remove all residual metal and organic contaminants before considered suitable for use.

4.2 Sample preparation

Prior to use in stock solutions, most salts were treated to remove trace surface active organic residues. The filtration of salt solutions was required, as it has been shown[63] that solutions made with ACS grade salts (≥99% purity) still contain trace amounts of surface-active organic impurities. The filtered solutions were then checked for impurities using vibrational sum frequency generation (VSFG) spectroscopy in the C−H stretching region (2800−3000 cm^{-1}). At the time of measurement, peaks associated with C−H stretching modes were observed (Appendix 2).

Salts with melting points greater than 650°C were baked in a high temperature oven to burn off organics, whereas lower melting point salts were filtered using active carbon filters (Whatman Carbon Cap 75, Fisher Scientific). Only NaCl and Na_2SO_4 had high enough melting points to be baked. The remainder were filtered at least three times. Mohr titration was used to determine the final concentration of the chloride stock solution. Raman spectroscopy was used to

determine the concentration of sulfate after filtration based on vibrational symmetric stretch of the ion (Appendix 3). Unlike salt solutions, know amounts of surfactants (SDS, CTAB) were weighed and dissolved directly with deionized water to make stock solutions and diluted to required concentration for use.

4.3 Experimental

Diluted salt solutions were carefully transferred into a clean Teflon dish via a glass pipette. It was assumed the surface was free of organic contaminants. With the platinum electrode fixed in place, the Am-241 was lowered to a height of 0.5 cm above the aqueous surface. A laser displacement sensor was used to confirm the relative height of the solution with an accuracy of ±0.03 cm relative to the sensor head. A specialized LabVIEW program was used to control the electrometer (sensitivity ± 0.001 mV). All SP measurements were taken under the following conditions: 20-21°C, 18-25% relative humidity, and 733.30-745.24 mm Hg barometric pressure.

Measurements made with this SP setup so far only focused on $E_{solution}$. In the initial fabrication of the setup, E_{water} was tested and found not to be reproducible. Since, several mechanical modifications were made to the setup but were tested solely with SDS and CTAB for reproducibility. Therefore, only $E_{solution}$ were collected and are reported in this study. In measuring $E_{solution}$, all solutions were measured in order of increasing concentration from one solution to the next. Despite taking the precaution of repeating experiments at the same time of day and within a close number of days, there were some repeatability errors. Both CTAB and SDS produced signals ±50 mV from one set of concentrations to another. Inorganic salts

produced signals that occasionally varied ±100 mV from one set of concentrations to the next. The reason for this is not clear. The potentials reported were of experimental sets closest to each other.

The LabVIEW program was designed to operate the Keithley 6517B and to collect data. The data parameters set were buffer size and measurement delay. Setting both in tandem determined the collection time for the experiment. For example, a buffer size of 2400 with a measurement delay of 375ms had an experiment time of 20 min. Once the electrometer collected the data, it would dump into the LabVIEW program where it could be exported. A typical runtime for the experiment depended on the rise time of the electrometer (Figure 4.1). For these experiments, the average runtime was 3-7 minutes to achieve the plateau potential response. The potential data used for analysis was the average from the maximum plateau region of the raw signal.

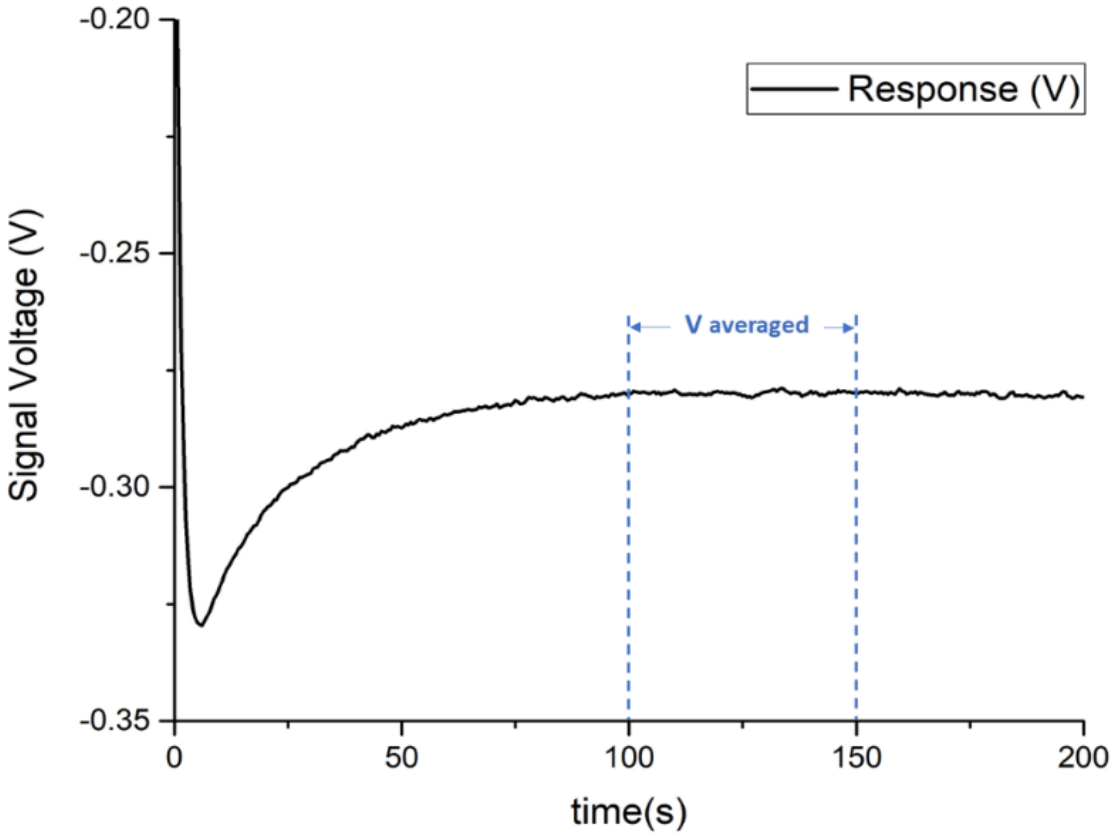

Figure 4.1 Instrument response for 1.5M $MgCl_2$ (ionizing probe height: 0.5 cm). In this case, the raw signal from 100-150s would be averaged and used for analysis.

CHAPTER 5 RESULTS AND DISCUSSION

5.1 Surface potential of charged surfactants

Heterodyne-detected vibrational sum frequency (HD-VSFG) of charged surfactants sodium dodecyl sulfate (SDS) and cetyl trimethylammonium bromide (CTAB) show how water molecules orient hydrogens up at the negatively charged aqueous interface and oxygen up at the positively charged aqueous interface.[55] Comparatively, measured surface potential of SDS[64] and CTAB[65] also show differences in sign and magnitude which indicate flip-flopping of water molecules based on surface charge. Results from this study agree with previous findings by others and validate the functionality of the SP setup.

For clarification, the surfactants potentials measured by the SP setup are $E_{solution}$. The potentials they compared to are ΔV, which is the difference in measured potentials of $E_{solution+water}$ and $E_{pure\ water}$. Since $E_{pure\ water}$ is constant between varying concentrations of subphase, the measured $E_{solution}$ is consistent with the increasing ΔV trend observed for the pre-critical micelluar concentrations (CMC) of both surfactants. The $E_{surfactant+water}$ values were measured directly with SP (Table 5.1) and compared with ΔV by Nakahara et al., (2005)[64] and Nakahara et. al., (2008)[66] in Figure 5.1 and Figure 5.2 respectively.

There were some experimental differences between Nakahara and this study. Though both studies utilize an americium based ionizing probe, Nakahara does not specify the activity of their experimental probe. Another difference was the use of a titration method to slowly increase the concentration of surfactant bulk by Nakahara. Doing this meant several adjustments to the height of the ionizing probe during the course of their experiments. Despite these differences,

Nakahara was able to reproduce their results by ±5 mV. For the SP experiments with both SDS and CTAB, the average standard deviation was approximately ±30mV. It is not clear how such high standard deviations might exist for these apart from the possibility of surface contamination after solutions were deposited into the dish. For these experiments, no surface cleaning procedure was used after the solution was placed into the petri dish. Despite this, the results shown strongly correlate with the Nakahara studies in trend and sign.

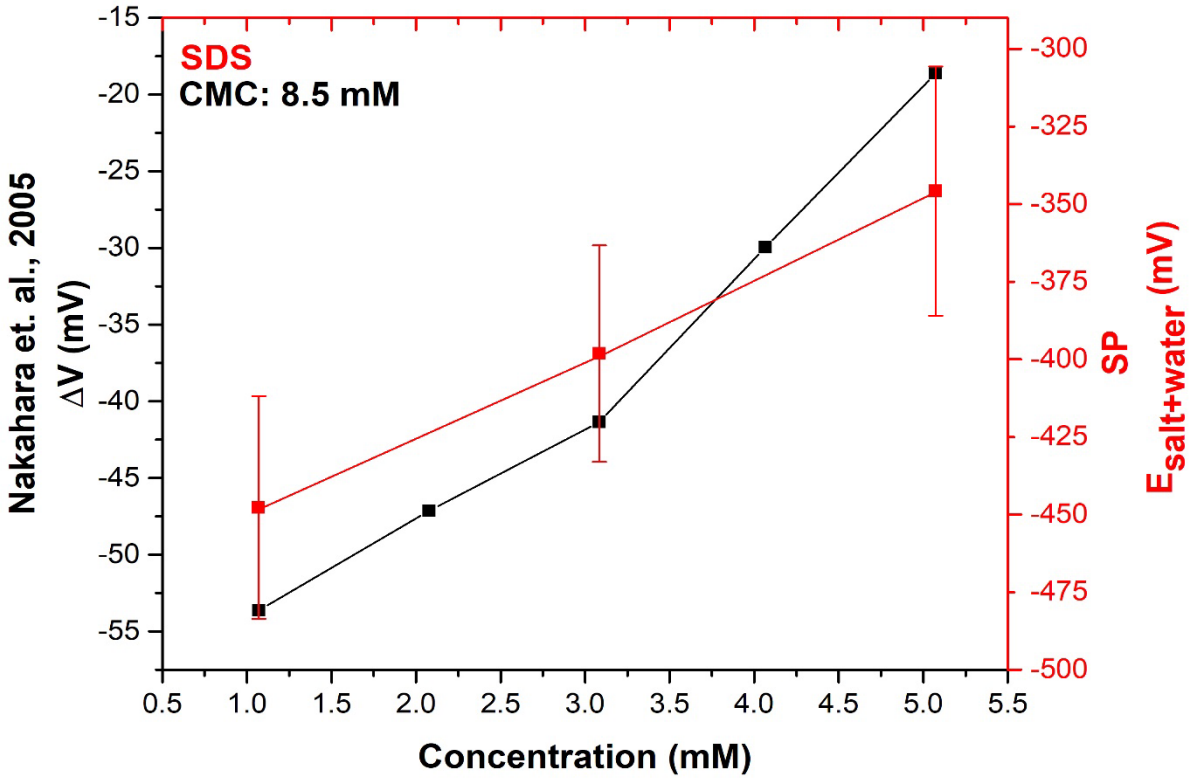

Figure 5.1 Comparison of ΔV_{SDS} with $E_{SDS+water}$. Error bars represent the standard deviation for n = 4.

As observed in these figures, the general trend of potentials was an increase from lower concentrations to a higher concentration. For SDS, ΔV_{SDS} has a linear increase from 1 to 3mM and another sharper increase from 3 to 5mM. One should note the CMC of SDS is 8.5mM. Thus, for this concentration range, the SDS molecules are arranged as monolayers at the surface. A similar trend to ΔV_{SDS} is observed for CTAB. Apart from the obvious difference that has a larger ΔV, the increase from 0.8 to 1.0 mM occurs over the CMC (0.92 mM). From Figure 5.1, $E_{SDS+water}$ observed to follow the trend of increase in potential across this concentration while consistently detecting the negative potential values for each concentration. Similarly, Figure 5.2 shows CTAB increasing across the concentration range while measuring positive potential values.

Considering the structure of SDS (Figure 5.3), the magnitude of measured ΔV_{SDS} depends on several components[67]: electrostatic interactions of the charged head groups (hydrophilic region), the dipole moments of the sulfate, ammonium in the head group, and the terminal CH chain (hydrophobic region), and change in dipole moment of associated water molecules. With increasing concentration of SDS, the number of charged groups at the surface is expected to result in a greater decrease of ΔV_{SDS} until a saturation point (CMC) is reached and the ΔV measured is limited by the surface area. Interestingly, ΔV_{SDS} measurements of the 1-7 mM concentration regime of SDS show a slight increase in potential. The authors argue this increase is the result of increasing Na^+ near the interface; electrostatically attracted to the negative surface and slightly neutralizing the surface charge, which is measured by the increasing ΔV_{SDS} below the CMC. In a similar mechanism, Br^- is electrostatically attracted to the positive

CTA^+ surface but does not appear to affect the large excess of CTA^+ and the dipole moments of the long hydrophobic alkyl-chain (Figure 5.3).

Putting ΔV_{SDS} to one side, the actual sign of the measured potentials is used to determine orientation of interfacial water molecules as described in Section 3.2.3. According to Gibbs adsorption theory, DS^- is preferentially adsorbed at the interface as it drastically decreases the surface tension of pure water (72 mN/m at 25 °C) to 25 mN/m.[68] Comparatively, NaCl only slightly increases surface tension.[69] Because DS- is negatively charged and adsorbs at the

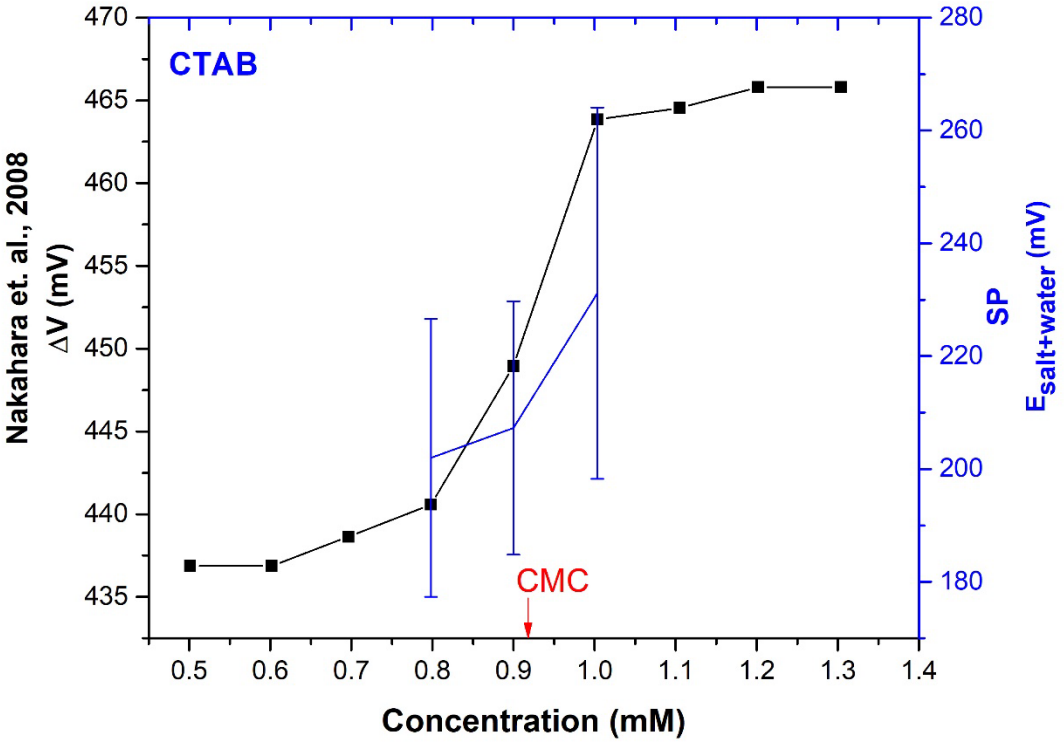

Figure 5.2 Comparison of ΔV_{CTAB} with $E_{CTAB+water}$. Error bars represent the standard deviation for n = 3.

interface, it follows that it wholly dominates the mostly neutral water surface. Now consider how the directly measured $E_{SDS+water}$ have a negative sign. This is a directly observable macroscopic phenomenon, implying that the dipoles of water orient hydrogens up towards the negative interface which has been confirmed by HD-VSFG studies mentioned earlier. In a similar way, $E_{CTAB+water}$ has a positive sign indicating a positive surface charge. From 1mM to 5mM, $E_{SDS+water}$ had a negative sign but had a positive trend. This shows that while Na^+ has an effect on the interfacial layer, DS^- is obviously the dominant species at the interface.

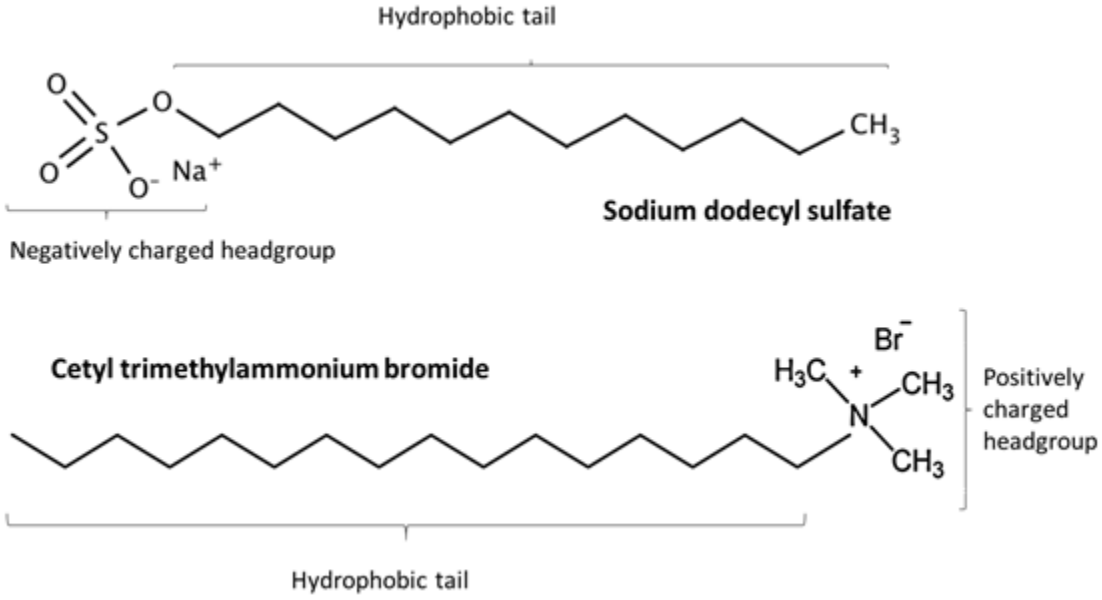

Figure 5.3 Structures of SDS and CTAB.

Table 5.1 *Summary of potential data collected by SP and compared to Nakahara et. al., 2005[*] and Nakahara et. al., 2008[+]. 'n' represents the average number of trials for* $E_{surfactant}$*. The error shown is the standard deviation.*

SDS (n = 4)			**CTAB (n = 3)**		
Conc. (mM)	$^{*}\Delta V$ (mV)	$E_{SDS+water}$ (mV)	Conc. (mM)	$^{+}\Delta V$ (mV)	$E_{CTAB+water}$ (mV)
1.0	-54	-447.9 ± 35.8	0.8	+440	+202.1 ± 24.6
3.0	-41	-398.5 ± 34.8	0.9	+448	+207.5 ± 22.4
5.0	-19	-346.1 ± 40.1	1.0	+463	+231.4 ± 32.9

5.2 Surface potential of inorganic electrolytes

In reviewing the currently available set of surface potential data for electrolytes, it is apparent that the accuracy and reproducibility of these experiments is quite challenging.[51] Apart from the obvious problems of controlling any surface contamination of water, salts, and/or equipment, there are too many variations in measured surface potential values of neat water and electrolytes. This may partly be due to non-standardization of experimental parameters and variance in experimentation method.[51] From review of literature, it appears that experimental surface potential values tend to fall within ±200mV. In the second half of this study, the goal was to reproduce the magnitude and trends of electrolytes from the 1968 Jarvis-Scheiman[17] paper on the $E_{salt+water}$ for several inorganic electrolytes. This study shows agreement in sign and relative magnitude for the various salts, but fails to fall within range of their values.

Four salts (NaCl, Na_2SO_4, $MgCl_2$, $MgSO_4$) were selected to reproduce results from the Jarvis-Scheiman study. The change in surface potential due to electrolytes is plotted as a function of concentration (moles/kg water) in Figure 5.4. In this figure, the filled symbols are data from this SP setup. The open symbols are from Jarvis-Scheiman. The $E_{salt+water}$ plotted was determined by successive dilutions of salt stock solutions. From the potential values obtained, a linear fit curve was obtained and extrapolated to zero-concentration. The reported surface potential values are differences of the zero-concentration potential and the potentials measured at the marked concentration ($\Delta E_{salt+water}$). Because the reference potential of the Am-241 is unknown, the zero-concentration potential is not equivalent to the surface potential of bare water. Results are summarized in Table 5.2.

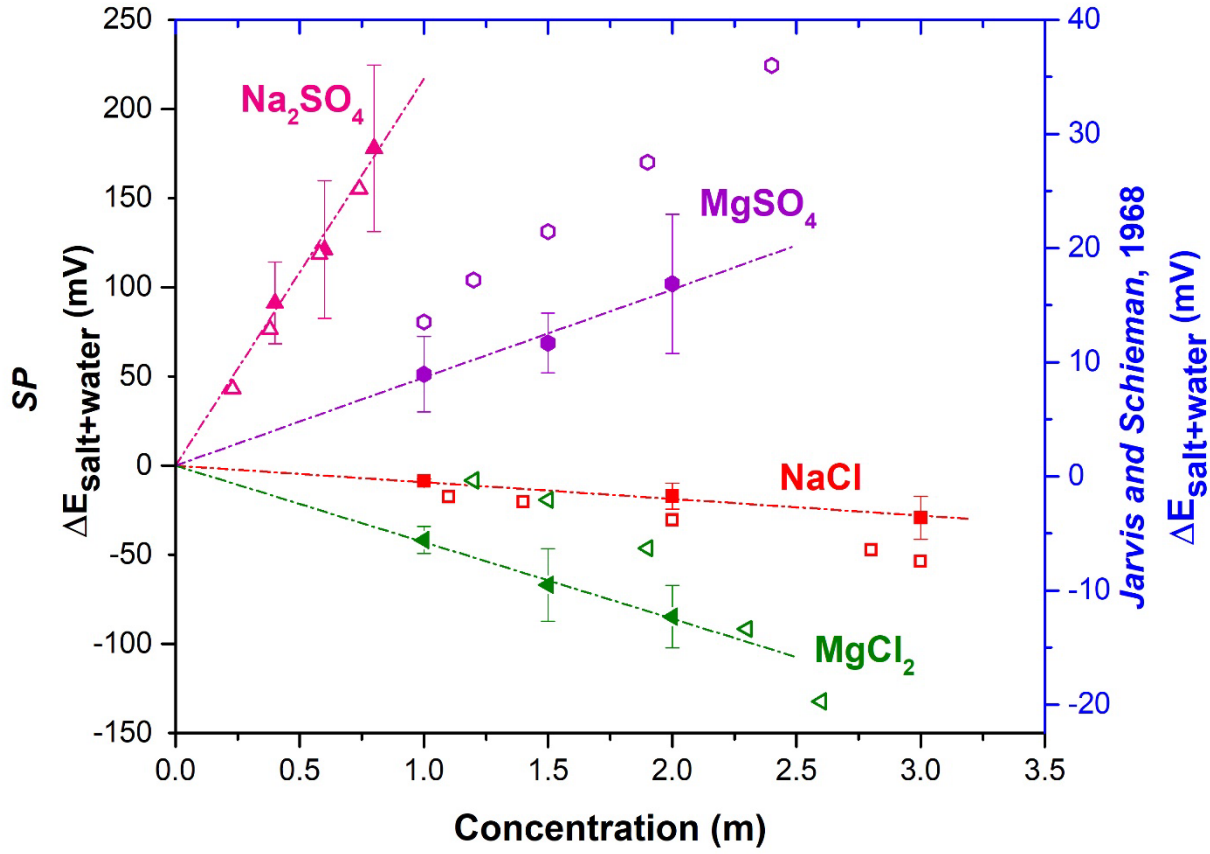

Figure 5.4 Comparision of values from Jarvis and Schieman (open symbols) and SP (filled symbols)

On the experimental plane of differences, the Jarvis and Scheiman study used a Polonium-210 based ionization source. Several procedures were implemented to remove organic contamination, including the use of large petri dishes with wax-lined rims. The surface was swept with waxed glass barriers to remove all signs of contamination. A Teflon-covered magnetic stir bar was used to keep the solutions uniform. These measures were not used for this study and may have contributed to the exceptionally large standard deviations reported.

As observed in Figure 5.4, there are several important observations to be made. First, between Na and Mg, the magnitude depends on the anion: SO_4^{2-} causes a positive shift, whereas Cl^- causes a negative shift. Compared to NaCl, it appears that increasing the $MgCl_2$ concentration tends results in greater difference in magnitude between the two salts. Additionally, $E_{salt+water}$ were measured as negative potentials (Table 5.2). These observations point to a fundamental discovery about salt solutions and their impact on the air/water interface. The positive $\Delta E_{salt+water}$ seems to indicate salts which prefer bulk over surface, whereas the negative $\Delta E_{salt+water}$ trend indicates that these salts also have some propensity for the surface.

Molecular Dynamics (MD) simulation study by Jungwirth and Tobias[21] provided a revolutionary revision to the historic understanding of ions being expelled from the air/water interface. Their model showed large halide ions (Br^-, I^-) as having a high propensity for the surface, despite maintaining a negative surface excess based on its ionic distribution. This was soon after confirmed by several techniques. However, this opened the door to exploring the physical reasons for ion specificity at the aqueous interface. The 1968 study by Jarvis and Scheiman provided insight into this from the trends and relative magnitudes of the $E_{salt+water}$. A density profile study of NaCl and HCl showed surface preference of Cl^-.[23] From looking at their surface tension profiles, however, the surface propensity of NaCl could not have been predicted as it behaves like a typical salt and raises the surface tension of water. Comparatively, ΔV of salts has been generally interpreted as exhibitive of the EDL near the surface[15], in that anions are closer to the interface than the cations, MD simulations confirm this picture to show that halides have preference to the surface in an order: $Cl^- < Br^- < I^-$. Other MD simulations by

Morita et. al.[70,71] explored distributions of $NaSO_4$ and H_2SO_4 only to show these ionic species to be repelled from the interface. Jungwirth[72] proposed that SO_4^{2-} prefers bulk over surface solvation; SO_4^{2-} is strongly being repelled from the surface, increasing the thickness of the interfacial region.

Based on the large difference in magnitude of Mg salts from Na salts was first attributed to the EDL by Jarvis and Scheiman[17] and Randles[15] based on their interpretation of surface potential. Only more recently MD simulations[24] show the $MgSO_4$ and $MgCl_2$ to form solvated ion pairs (SIPs) on the interface. SIPs affect distribution of cations and anions in the EDL. For $MgCl_2$, the Cl^- is preferential to the surface, thereby creating an EDL distribution of anions followed by cations. This correlates with the negative $\Delta E_{salt+water}$ trend for $MgCl_2$ with water molecules oriented hydrogen up towards the interface. On the other hand, aqueous $MgSO_4$ did the opposite since SO_4^{2-} is repelled from the interface, whereby Mg^{2+} are forced towards the interface causing it to become positively charged. Again, this correlates to the positive $\Delta E_{salt+water}$ trend observed for $MgSO_4$. The importance of these results can be discounted as these studies correlate to show the influence of ions on interfacial water at the EDL.

Table 5.2. Data of surface potential difference (n = 5).

Conc. (m)	***NaCl***	
	$E_{salt+water}$	$\Delta E_{salt+water}$
1.0	-401.97 ± 76.84	-10.33 ± 1.14
2.0	-408.84 ± 76.15	-17.20 ± 7.26
3.0	-420.89 ± 77.09	-29.25 ± 12.10
T (°C)	22.0 ± 0.1	
RH (%)	18.4 ± 1.1	

Conc. (m)	***Na_2SO_4***	
	$E_{salt+water}$	$\Delta E_{salt+water}$
0.4	-452.16 ± 50.56	91.26 ± 23.02
0.6	-422.35 ± 38.91	121.07 ± 38.58
0.8	-365.42 ± 31.81	178.00 ± 46.71
T (°C)	22.0 ± 0.1	
RH (%)	19.4 ± 1.1	

Conc. (m)	***$MgCl_2$***	
	$E_{salt+water}$	$\Delta E_{salt+water}$
1.0	-229.54 ± 15.95	-41.76 ± 7.55
1.5	-254.61 ± 23.58	-66.83 ± 20.35
2.0	-272.50 ± 20.56	-84.72 ± 17.49
T (°C)	21.4 ± 0.1	
RH (%)	18.2 ± 1.9	

Conc. (m)	***$MgSO_4$***	
	$E_{salt+water}$	$\Delta E_{salt+water}$
1.0	-451.99 ± 22.10	-51.18 ± 21.19
1.5	-427.93 ± 17.65	-68.75 ± 16.73
2.0	-401.25 ± 33.96	-101.93 ± 38.97
T (°C)	22.0 ± 0.1	
RH (%)	18.4 ± 1.1	

CHAPTER 6 CONCLUSION AND FUTURE WORK

6.1 Conclusion

This thesis is the output of building a refined analytical surface potential instrument in the Allen research laboratory. An americium-241 foil (20μCi, 9.5mm surface diameter) is suspended in the air above the sample solution and a platinum gauze electrode is placed into the solution below. These electrodes were connected to a Keithley 6517B electrometer directly. With this custom instrument, surface measurements of charged surfactants (SDS, CTAB) and inorganic electrolytes (NaCl, $MgCl_2$, Na_2SO_4, $MgSO_4$) were made. The results were compared to studies by Nakahara et. al, (2005, 2008) and Jarvis and Scheiman (1968).

Potentials measured for SDS and CTAB were observed to have a linear increase in concentration regimes below the critical micellular concentrations. The signs of the potentials observed were also consistent with the known surface charges for both molecules, and are consistent with findings by Nakahara. For inorganic salts, the surface potential difference versus concentration is plotted from 1-3m and extrapolated to zero concentration. Linear positive trends are observed for Na_2SO_4 and $MgSO_4$ whereas as a linear negative trend is observed for NaCl and $MgCl_2$. The magnitude of the potentials measured did not fall in range of the Jarvis-Scheiman study. Regardless, these results are consistent with theoretical analysis of ions at the air/water interface, both in terms of surface propensity and the effect on the EDL.

These results validate surface potential as a reasonable method for the study of molecules at the air/water interface. Future studies involving surface potential will provide insight on behavior of molecules with respect to interfacial water and other molecules.

6.2 Future Work

Based on the outcomes of this study, there are several modifications which are essential for future studies. First, a surface cleaning method must be used to obtain more reliable data. This may be achieved by a sweeping a waxed barrier on the surface or, alternatively, with the design of a new sampling dish with a waxed rim to attract organic and dust contaminants Second, the dependence of the height of the ionizing probe relative to the surface of subphase is known but not further clarified for repeatability of data. Though the probe was fixed for this study, the appropriate distance for measurement is not known. We believe this would matter greatly for future SP measurements as the probe height does play a vital role in the measured voltage for any substance at the interface. Third, and most important, is to continue to study various aqueous salts including complex ones, such as ferric chloride and copper chloride. Their effect on interfacial water is not well-understood but is extremely relevant to atmospheric processes and electrochemical applications. In conjunction with other microscopic techniques, such as vibrational sum frequency generation and second harmonic generation, SP proves to be a vital technique in assessing behavior of ions at the air/water interface.

Appendix

1. Calculation of the Extent of Air Ionization from the Americium-241

An estimate of the extent of air ionization from the Americium-241 (20 µCi, 9.5 mm active diameter) is calculated based on experimental parameter of these experiments. It was assumed that the flux of alpha particles emitted were uniform. Because the experiments were kept under a nitrogen purge, the energy for the formation of ion pairs used was 27.5eV.[73]

Strength of ionizing source = $20\ \mu Ci$

$$= (20 * 10^{-6}\ Ci)(37 * 10^{10}\ s^{-1}Ci^{-1})$$

$$= 7.4 * 10^{6}\ alpha\ particles\ s^{-1}$$

Volume of uncontained air directly under the active surface diameter (9.5 mm) of Am-241 probe at a height of 0.5cm above solution:

$$= 0.5\ cm * \ \pi(0.95\ cm)^2$$

$$= 1.416\ cm^3$$

Number of air molecules present at 20°C and 1 atm:

$$= \frac{PVN_A}{RT}$$

$$= \frac{(1.013 * 10^5)(1.416 * 10^{-6})(6.022 * 10^{23})}{(8.314)(293.15)}$$

$$= 3.54 * 10^{19}$$

Total energy of each α-particle at point of emission = $4.7\ MeV$

Number of ion pairs formed per α-particle (in nitrogen):

$$= \frac{E_0}{W}$$

$$= \frac{4.7 * 10^5 eV}{27.5 eV/pair}$$

$$= 1.71 * 10^4$$

Total number of ion pairs formed per second:

$$= (1.71 * 10^4)(7.4 * 10^6)$$

$$= 1.3 * 10^{11}$$

Total number of ions formed per second:

$$= (2)(1.3 * 10^{10})$$

$$= 2.53 * 10^{11}$$

The constant rate of ion production is N_0,

$$N_0 = \frac{2.53 * 10^{11}}{1.53}$$

$$= 1.65 * 10^{11}\ ions\ s^{-1}\ cm^{-1}$$

The rate of recombination of ionized particle as demonstrated by Rutherford[74], where *n* is the number of ions/cm^3, *t* is seconds, and $\alpha = 1.60 * 10^{-6}$:

$$\frac{dn}{dt} = -\alpha n^2$$

$$\frac{dn}{dt} = N_0 - 1.60 * 10^{-6} n^2$$

Solving for *n* results in the expression,

$$n = \frac{\left(-1\sqrt{1 + 4\alpha t^2 N_0}\right)}{2\alpha t}$$

The steady concentration of ions is:

$$n = \sqrt{\frac{N_0}{\alpha}}$$

$$= \sqrt{\frac{1.65 * 10^{11}}{1.60 * 10^{-6}}}$$

$$= 3.2 * 10^8 \; ions/cm^3$$

The total number of ions present is:

$$= (3.2 * 10^8)(1.53)$$

$$= 4.90 * 10^8 \; ions$$

Therefore, the percentage of air molecules ionized:

$$= \frac{4.90 * 10^8}{3.54 * 10^{19}} \text{ x } 100$$

$$= \mathbf{1.38 * 10^{-9}}\%$$

2. VSFG testing of organic contaminants

Using a custom-built VSFG spectroscopy system available in the Allen lab, a test for organic contamination of salts solutions were made with assistance of Dr. Lin Lu.

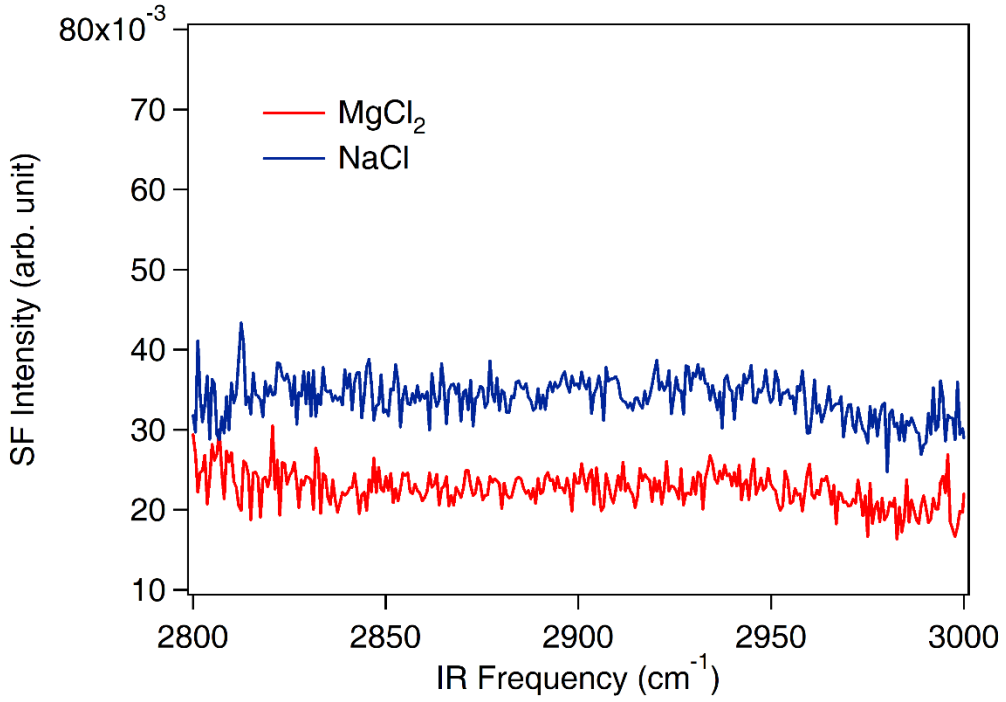

Figure A.1: Vibrational sum frequency spectra of salts NaCl and $MgCl_2$. Courtesy of Dr. Lin Lu.

3. Raman spectroscopy of $MgSO_4$

The peak intensities from the vibration symmetric sulfate band were measured using an Acton LS-785 NIR Raman coupled with a PIXIS CCD detector from Princeton Instruments PIXIS. By considering these intensities as a function of concentration (Beer's law), the unknown concentration of $MgSO_4$ was determined after filtration. The results are shown in the graph below.

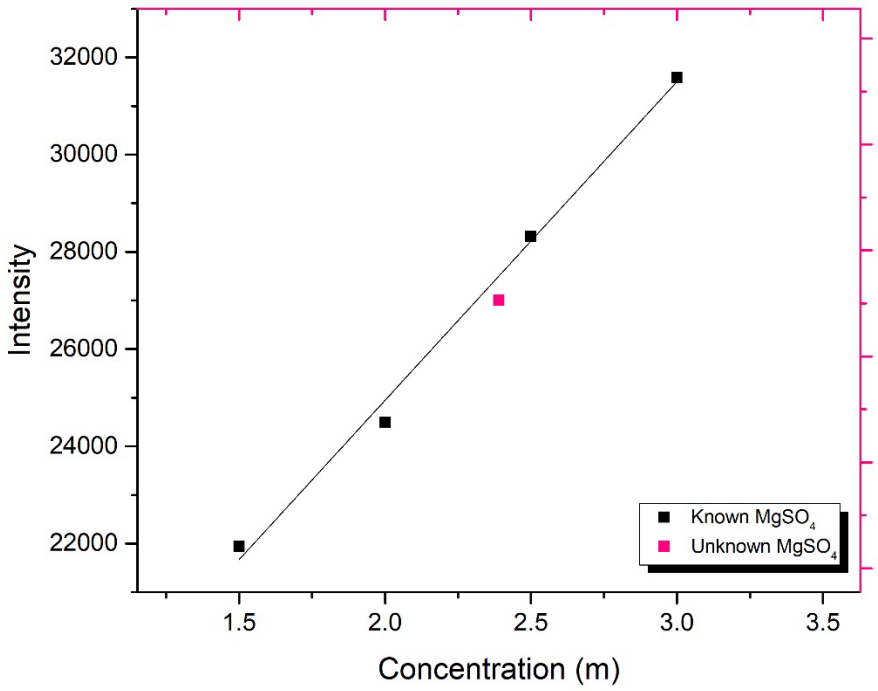

Figure A.2: Graph of intensity versus concentration for $MgSO_4$ solutions.

Intercept	11837.4 ± 7.94E+02
Slope	6553.6 ± 3.43E+02
Residual Sum of Squares	2.93E+05
Pearson's r	9.97E-01
R-Square (COD)	9.95E-01
Adj. R-Square	9.92E-01

References

1. Girault, H. H. Analytical and Physical Electrochemistry. *EPFL Press*: New York, **2004**.
2. Piazza, R. *J. Cryst. Growth.* **1999**, 196**,** 415–423.
3. Cacace, M. G.; Landau, E. M.; Ramsden, J. J. *Q. Rev. Biophys.* **1997**, 30**,** 241–277.
4. Tavares, F. W.; Bratko, D.; Prausnitz, J. M. *Curr. Opin. Colloid Interface Sci.* **2004**, 9, 81–86.
5. Gradzielski, M. *Curr. Opin. Colloid Interface Sci.* **2004**, 9, 256–263.
6. Millero, F. J.; Feistel, R.; Wright, D. G.; McDougall, T. J. *Deep Sea Res. Part Oceanogr. Res. Pap.* **2008**, 55, 50–72.
7. Shcherbina, A. Y.; Talley, L. D.; Rudnick, D. L. *Science.* **2003**, 302, 1952–1955.
8. Jungwirth, P.; Rosenfeld, D.; Buch, V. *Atmospheric Res.* **2005**, 76, 190–205.
9. Heydweiller, A. *Ann Phys.* **1910**, 33, 145–185.
10. Langmuir, I. *J. Am. Chem. Soc.* **1917**, 39, 1848–1906.
11. Wagner, C. *Phys. Z.* **1924**, 25, 474–477.
12. Onsager, L.; Samaras, N. N. T. *J. Chem. Phys.* **1934**, 2, 528–536.
13. Levin, Y.; Flores-Mena, J. E. *Eur. Lett.* **2001**, 56, 187.
14. Frumkin, A. *Z. Phys. Chem.* **1924**, 109, 34–48.
15. Randles, J. E. B. *Discuss. Faraday Soc.* **1957**, 24, 194–199.
16. Randles, J. E. B.; Schiffrin, D. J. *J. Electroanal. Chem. (1959)* **1965,** 10**,** 480–484.

17. Jarvis, N. L.; Scheiman, M. A. *J. Phys. Chem.* **1968**, 72, 74–78.

18. Jarvis, N. L. *J. Geophys. Res.* **1972**, **77,** 5177–5182.

19. Randles, J. E. B. *Phys. Chem. Liq.* **1977**, **7,** 107–179.

20. Durand-Vidal, S.; Simonin, J.-P.; Turq, P. *Electrolytes at Interfaces*. Springer Science: Netherlands, **2000**.

21. Jungwirth, P.; Tobias, D. J. *J. Phys. Chem. B.* **2001**, 105, 10468–10472.

22. dos Santos, A. P.; Diehl, A.; Levin, Y. *Langmuir*. **2010**, 26, 10778–10783.

23. Jungwirth, P.; Tobias, D. J. *Chem. Rev.* **2006**, 106, 1259–1281.

24. Götte, L.; Parry, K. M.; Hua, W.; Verreault, D.; Allen, H. C.; Tobias, D. J. *J. Phys. Chem. A* **2017**, 121, 6450–6459.

25. Zhou, J.; Santambrogio, G.; Brummer, M.; Moore, D. T.; Meijer, G.; Neumark, D. M.; Asmis, K. R.; Woste, L. *J. Chem. Phys.* **2006**, 125, 111102.

26. Xu, M., Larentzos, J. P., Roshdy, M., Criscenti, L. J.; Allen, H. C. *Phys. Chem. Chem. Phys.* **2008**, 10, 4793–4801.

27. Randles, J. E. B.; Delahay, P. Tobias, C. W. *Advances in Electrochemistry and Electrochemical Engineering, Vol. 3*, Interscience: New York, **1962**.

28. Parsons, R. *Can. J. Chem.* **1959**, 37, 308–314.

29. Bard, A. J.; Faulkner, L. R. *Electrochemical Methods: Fundamentals and Applications, Vol. 2,* Wiley: New York, **2000**.

30. Cohen, E. Richard, ed. *Quantities, units and symbols in physical chemistry*. Royal Society of Chemistry London, **2007**.

31. Aveyard, R.; Haydon, D. A. *An Introduction to the Principles of Surface Chemistry*. Cambridge University Press: London, **1973**.
32. Demchak, R. J.; Fort, T. *J. Colloid Interface Sci.* **1974**, 46, 191–202.
33. Petrov, J. G.; Polymeropoulos, E. E.; Möhwald, H. *J. Phys. Chem.* **1996**, 100, 9860–9869.
34. Casper, C. B.; Verreault, D.; Adams, E. M.; Hua, W.; Allen, H. C. *J. Phys. Chem. B.* **2016**, 120**,** 2043–2052.
35. Darlington, A. M.; Jarisz, T.A.; DeWalt-Kerian, E.L.; Roy, S.; Kim, S.; Azam; M.S.; Hore, D.K.; Gibbs, J.M., *J. Phys. Chem. C.* **2017**, 121**,** 20229–20241.
36. Allongue, P. *Phys. Rev. Lett.* **1996**, 77, 1986–1989.
37. Velasco-Velez, J.J.; Wu, C. H.; Pascal, T. A.; Wan, L. F.; Guo, J.; Prendergast, D.; Salmeron, M. *Science.* **2014**, 346**,** 831–834.
38. Lis, D.; Backus, E. H. G.; Hunger, J.; Parekh, S. H.; Bonn, M. *Science.* **2014**. 344**,** 1138–1142.
39. Gragson, D. E.; McCarty, B. M.; Richmond, G. L. *J. Am. Chem. Soc.* **1997**, 119**,** 6144–6152.
40. Guggenheim, E. A. *Trans. Faraday Soc.* **1940**, 35**,** 397–412.
41. Kathmann, S. M.; Kuo, I.-F. W.; Mundy, C. J.; Schenter, G. K. *J. Phys. Chem. B.* **2011**, 115**,** 4369–4377.
42. Israelachvili, J. N. *Intermolecular and Surface Forces*. Academic Press, Boston: **2011**.
43. Guyot, J. *Ann Phys.* **1924**. 506–638.
44. Schulman, J. H.; Rideal, E. K. *Proc. R. Soc. Lond. Ser. Contain. Pap. Math. Phys. Character* **1931**, 130**,** 259–270.

45. Bockris, J. O.; Conway, B. E. *Modern Aspects of Electrochemistry*. Plenum Press: New York, **2012**.
46. Barzyk, W.; Vuorinen, J. *Colloids Surf. Physicochem. Eng. Asp.* **2011**, 385**,** 1–10.
47. Fatihou, A.; Dascalescu, L.; Zouzou, N.; Dumitran, L. M. *2014 IEEE Industry Application Society Annual Meeting*, **2014**, 1–6.
48. Burdon, R. S. *Surface Tension and the Spreading of Liquids*. Cambridge University Press: Cambridge, **2014**.
49. Llopis, J. *Modern Aspects of Electrochemistry No. 6*, 91–158. Springer: Boston: **1971**.
50. Parsons, R. *Modern aspects of electrochemistry: No. 29*, Plenum Press: New York, **1997**.
51. Verreault, D.; Allen, H. C. *Chem. Phys. Lett.* **2013**, 586**,** 1–9.
52. Perakis, F. *et al.* **2016**, 116, 7590–7607.
53. Schnitzer, C.; Baldelli, S.; Shultz, M. J. *J. Phys. Chem. B.* **2000**, 104**,** 585–590.
54. Bockris, J. *Modern Electrochemistry: An Introduction to an Interdisciplinary Area*. Springer Science: Netherlands, **2012**.
55. Nihonyanagi, S.; Yamaguchi, S.; Tahara, T. *J. Chem. Phys.* **2009**, 130**,** 204704.
56. N. K. Adam. The physics and chemistry of surfaces. Oxford University Press: London, **1938**.
57. Kirk, D. W.; Foulkes, F. R. *J. Electrochem. Soc.* **1984**, 131**,** 1332–1336.
58. Wood, M. J. *Platinum Metals Rev.* **1966**, 10, (4).
59. *Low Level Measurements Handbook: Precision DC Current, Voltage, and Resistance Measurements*. Keithley/Tektronix. **2016**.
60. Pfeiffer, J. C. *Principles of Electrical Grounding*. **2001**.

61. Gaines, G. L. *Insoluble monolayers at liquid-gas interfaces*. Interscience Publishers: **1966**.
62. Seaborg, G. T. *Nucl. Sci. Eng.* **1961**, 9, 475–487.
63. Hua, W.; Verreault, D.; Adams, E. M.; Huang, Z.; Allen, H. C. *J. Phys. Chem. C.* **2013**. 117, 19577–19585.
64. Nakahara, H.; Shibata, O.; Moroi, Y. *Langmuir*. **2005**, 21, 9020–9022.
65. Nakahara, H.; Shibata, O.; Moroi, Y. *J. Phys. Chem. B.* **2011**, 115, 9077–9086.
66. Nakahara, H.; Shibata, O.; Rusdi, M.; Moroi, Y. *J. Phys. Chem. C.* **2008**, 112, 6398–6403.
67. Dragčević, Đ.; Bujan, M.; Grahek, Ž.; Filipović-Vinceković, N. *Colloid Polym. Sci.* **1995**, 273**,** 967–973.
68. Birdi, K. S. *Introduction to Electrical Interfacial Phenomena*. CRC Press: Boca Raton, **2010**.
69. Chattoraj, D. K.; Birdi, K. S. *Adsorption and the Gibbs surface excess*. Plenum Press: New York, **1984**.
70. Ishiyama, T.; Morita, A. *J. Phys. Chem. C.* **2011**, 115**,** 13704–13716.
71. Ishiyama, T.; Morita, A.; Miyamae, T. *Phys. Chem. Chem. Phys. PCCP*. **2011**, 13**,** 20965–20973.
72. Jungwirth, P.; Curtis, J. E.; Tobias, D. J. *Chem. Phys. Lett.* **2003**. 367**,** 704–710.
73. Binks, W. *Acta Radiol.* **1954**, 42**,** 85–104.
74. Rutherford, E. *Radioactive Substances and Their Radiations*. University Press: New York, **1913**.